Article:

Faruq, N.Z. and Susmel, L. (2019) Proportional/non-proportional constant/variable amplitude multiaxial notch fatigue: cyclic plasticity, non-zero mean stresses, and critical distance/plane. Fatigue and Fracture of Engineering Materials and Structures, 42 (9). pp. 1849-1873. ISSN 8756-758X

https://doi.org/10.1111/ffe.13036

Proportional/non-proportional constant/variable amplitude multiaxial notch fatigue: cyclic plasticity, non-zero mean stresses, and critical distance/plane

N. Zuhair Faruq and Luca Susmel

Department of Civil and Structural Engineering, The University of Sheffield, Mapping Street, Sheffield S1 3JD, UK

Corresponding Author: Prof. **Luca Susmel**
Department of Civil and Structural Engineering
The University of Sheffield, Mappin Street, Sheffield, S1 3JD, UK
Telephone: +44 (0) 114 222 5073
Fax: +44 (0) 114 222 5700
e-mail: l.susmel@sheffield.ac.uk

Abstract
This paper deals with the formulation and experimental validation of a novel fatigue lifetime estimation technique suitable for assessing the extent of damage in notched metallic materials subjected to in-service proportional/non-proportional constant/variable amplitude multiaxial load histories. The methodology being formulated makes use of the Modified Manson-Coffin Curve Method, the Shear Strain-Maximum Variance Method and the elasto-plastic Theory of Critical Distance, with the latter theory being applied in the form of the Point Method. The accuracy and reliability of our novel fatigue lifetime estimation technique were checked against a large number of experimental results we generated by testing, under proportional/non-proportional constant/variable amplitude axial-torsional loading, V-notched cylindrical specimens made of unalloyed medium-carbon steel En8 (080M40). Specific experimental trials were run to investigate also the effect of non-zero mean stresses as well as of different frequencies between the axial and torsional stress/strain components. This systematic validation exercise allowed us to demonstrate that our novel multiaxial fatigue assessment methodology is remarkably accurate, with the estimates falling within an error factor of 2. By modelling the cyclic elasto-plastic behaviour of metals explicitly, the design methodology being formulated and validated in the present paper offers a complete solution to the problem of estimating multiaxial fatigue lifetime of notched metallic materials, with this holding true independently of sharpness of the stress/strain raiser and complexity of the load history.

Keywords: Multiaxial fatigue, variable amplitude, notch, critical plane, critical distance.

NOMENCLATURE

b	Fatigue Strength Exponent
b_o	Shear Fatigue Strength Exponent
c	Fatigue Ductility Exponent
c_o	Shear Fatigue Ductility Exponent
f	ratio between the frequencies of the axial and torsional loading channels
n'	Cyclic Strain Hardening Exponent
n'_{NP}	Cyclic Strain Hardening Exponent under 90° out-of-phase loading
t	Time
$F_{a\text{-}max}$	Maximum amplitude of the axial force in the load history
K'	Cyclic Strength Coefficient
K'_{NP}	Cyclic Strength Coefficient under 90° out-of-phase loading
K_t	Linear-elastic stress concentration factor under axial loading
K_{tt}	Linear-elastic stress concentration factor under torsion
L	Critical distance
N_b	Number of blocks to failure
$N_{b,e}$	Estimated number of blocks to failure

N_f Number of cycles to failure
$N_{f,e}$ Estimated number of cycles to failure
Oxyz Frame of reference
r Notch root radius
R Load ratio
T Time length of the observation period
$T_{a\text{-}max}$ Maximum amplitude of the torsional force in the load history
δ Out-of-phase angle
ε'_f Fatigue Ductility Coefficient
$\varepsilon_{x,a}$ Amplitude of the axial strain
$\varepsilon_{x,a\text{-}max}$ Maximum amplitude of the axial strain in the load history
γ'_f Shear Fatigue Ductility Coefficient
$\gamma'_f(\rho)$ Multiaxial Fatigue Ductility Coefficient depending on ρ
γ_a Shear strain amplitude relative to the plane of maximum shear strain amplitude
γ_m Mean value of the shear strain relative to the critical plane
$\gamma_{MV,max}$ Maximum and minimum value of $\gamma_{MV}(t)$
$\gamma_{MV,min}$ Minimum value of $\gamma_{MV}(t)$
$\gamma_{MV}(t)$ resolved shear stain
$\gamma_{xy,a}$ Amplitude of the shear strain
$\gamma_{xy,a\text{-}max}$ Maximum amplitude of the shear strain in the load history
ν_e Poisson's ratio for elastic strain
ν_p Poisson's ratio for plastic strain
σ'_f Fatigue Strength Coefficient
$\sigma_n(t)$ Stress normal to the critical plane
$\sigma_{n,max}$ Maximum stress perpendicular to the critical plane
$\sigma_{n,min}$ Minimum stress perpendicular to the critical plane
σ_{UTS} Ultimate tensile strength
$\sigma_{x,a}$ Amplitude of the axial stress
ρ Stress ratio relative to the critical plane ($\rho=\sigma_{n,max}/\tau_a$)
ρ_{lim} Limit value for stress ratio ρ
τ'_f Shear Fatigue Strength Coefficient
$\tau'_f(\rho)$ Multiaxial Fatigue Strength Coefficient depending on ratio ρ
τ_a Shear stress amplitude relative to the critical plane
τ_m Mean value of the shear stress relative to the critical plane
$\tau_{MV,max}$ Maximum of resolved shear stress $\tau_{MV}(t)$
$\tau_{MV,min}$ Minimum value of resolved shear stress $\tau_{MV}(t)$
$\tau_{MV}(t)$ Resolved shear stress
$\tau_{xy,a}$ Amplitude of the shear stress

1. Introduction

In situations of practical interest engineering components and structures not only contain geometrical features leading to localised stress/strain concentration phenomena, but are also subjected to in-service variable amplitude multiaxial load histories. This explains why since the beginning of the last century a tremendous effort has been made worldwide to devise robust design methodologies suitable for addressing such an intractable problem.

In terms of fatigue assessment philosophies, examination of the state of the art demonstrates that so far the international scientific community has focussed their attention on the formulation of fatigue design parameters whose definition is based either on linear-elastic stresses or on elasto-plastic cyclic strains[1]. By their nature, stresses are usually preferred in those situations where cyclic plasticity can be neglected with little loss of accuracy - i.e., mainly in the medium/high-cycle fatigue regime[2]. In contrast, strains

are recommended to be used whenever metallic materials subjected to time-variable loading undergo large scale cyclic plastic deformations [3].
As far as notched components working in the medium/high-cycle fatigue regime are concerned, current state of knowledge shows that different multiaxial fatigue criteria have been devised by taking full advantage of the pioneering work done back in the 1940s-50s by Neuber [4] and Peterson [5]. In particular, these approaches model the detrimental effect of stress raisers either by performing the stress analysis in terms nominal quantities [6-9] or by directly post-processing the local linear-elastic stress/strain fields in the vicinity of the geometrical features under investigation [2, 10]. In this setting, the most successful criteria are seen to be those making use of either the critical plane concept [11-14] or energy related parameters [15-18].
As the magnitude of the forces/moments being applied increases, cyclic plasticity plays a role that becomes increasingly important [1-3]. This is the reason why under these circumstances the mechanical behaviour of metallic materials is no longer recommended to be modelled by using a simple linear-elastic constitutive law. By taking as a starting point this idea, in about the mid-50s Manson [19] and Coffin [20] proposed to estimate fatigue lifetime by making use of elasto-plastic cyclic strains. Subsequently, this approach was further developed by incorporating into it also the stress components, with this being done to model effectively the detrimental effect of superimposed static stresses [21, 22]. By forming the hypothesis that fatigue strength in the presence of notches is a function of the magnitude of the elasto-plastic root deformations, the strain based approach was subsequently extended also to the fatigue assessment of metallic components containing stress/strain raisers [1, 3]. In this context, the need for accurately quantifying root stresses and root strains explains why since the 1980s different attempts have been made to devise specific techniques suitable for estimating the elasto-plastic stresses and strains at the tips of notches [23-28].
As far as the multiaxial fatigue assessment problem is concerned, the use of root stresses and root strains applied in conjunction with the critical plane concept is seen to return accurate estimates [29-31]. This holds true provided that the structural details being designed are weakened by relatively blunt notches [30]. In contrast, when the notches under investigation are sharp, the strain based approach is seen to return results that are somehow too conservative, with the level of conservatism increasing as the sharpness of the stress/strain concentrators being assessed increases [32]. This explains the reason why notched components should be designed against fatigue by adopting suitable elasto-plastic fatigue strength reduction factors [1].
In order to extend effectively the use of the strain based approach also to those situations involving severe stress/strain gradients resulting from sharp geometrical features, in recent years a number of successful attempts have been made to develop design methodologies that couple local elasto-plastic stresses and strains with the so-called Theory of Critical Distances (TCD) [32-35]. The TCD is the name which has been given by David Taylor [10] to a group of methods that all use a material critical length to assess the strength of engineering components weakened not only by cracks, but also by short, sharp and blunt notches.
As to the use of the TCD as a structural design tool, it is worth observing here that, since the beginning of the 2000s, systematic theoretical/experimental work has been carried out to develop specific procedures suitable for using this theory along with the critical plane concept to perform, in the medium/high-cycle fatigue regime, the multiaxial fatigue assessment of notched components [11- 13, 36-38]. Thanks to this large body of work, nowadays we can make direct use of local linear-elastic stress fields to effectively design against proportional/non-proportional constant/variable amplitude uniaxial/multiaxial fatigue loading components containing geometrical features of all kinds [39, 40].
In this challenging scenario, owing to the accurate results that have been obtained in the recent past by applying the uniaxial elasto-plastic TCD [32, 33], this paper aims at extending in a rigorous and effective way the use of this theory to those notch situations involving cyclic elsto-plastic deformations and constant/variable amplitude multiaxial fatigue loading.

2. Theoretical framework

The methodology formulated and validated in the present paper makes use of the Modified Manson-Coffin Curve Method (MMCCM) [41, 42], the Shear Strain-Maximum Variance Method (γ-MVM) [42,

43] and the Theory of Critical Distance (TCD) [32, 33]. The MMCCM is an elsto-plastic critical plane approach whose formulation takes as a starting point the idea that fatigue damage reaches its maximum value on those material planes experiencing the maximum shear strain amplitude. According to the γ-MVM the orientation of the critical plane is determined via that direction which is associated with the maximum variance of the resolved shear strain. As far as variable amplitude load histories are concerned, this specific direction is used in conjunction with the standard Rain-Flow method also to count the fatigue cycles. In the presence of geometrical features, the detrimental effect of stress/strain gradients is modelled according to the Point Method (PM), i.e., by directly post-processing the stress/strain tensors at a given distance from the assumed crack initiation point. In this setting, the required critical distance is treated as a material property, with this characteristic length being closely related to the size of the dominant source of microstructural heterogeneity.
In what follows the key features of the different theories/approaches on which the proposed multiaxial fatigue design method is based are reviewed briefly.

2.1. Orientation of the critical plane and cycle counting

To estimate the orientation of those material planes experiencing the maximum shear strain amplitude, we have developed and systematically validated an efficient numerical tool [42, 43] that is based on the use of the maximum variance concept [44]. This section briefly summarises the key features of the γ-MVM, the reader being referred to Ref. [43] for the complete formulation of this methodology and its theoretical justification.
Initially, in order to clarify the fundamental idea on which the MVM is based, it is worth recalling here that the variance of a time-dependent signal is the average squared deviation of the signal itself from its mean value. Therefore, the variance can be thought of as a quantity that measures the amount of variation of the signal being assessed within the maximum and minimum values which define the absolute range. As far as fatigue assessment of metallic materials is concerned, this definition suggests that the variance of a stress/strain signal can be treated as a design quantity whose magnitude is proportional to the extent of the fatigue damage [42-44].
Another important implication associated with the way the variance is calculated is that the order of the cycles does not affect the way fatigue damage is quantified. In other words, in the presence a damaging event, the value of the calculated variance is in any case sensitive to this specific event, with this holding true no matter if this damaging event occurs at the beginning or at the end of the load history being assessed. In this setting, it is important to highlight that the sequence effect in the estimation of fatigue damage is taken into account instead via the specific hardening rule being employed to model/estimate the cyclic stress vs. strain response of the metal being designed.
Turning to the γ-MVM, this method defines the orientation of the critical plane via that direction, MV, that is associated with the maximum variance of the resolved shear strain, $\gamma_{MV}(t)$ – see Figs 1a and 1b. From a physical point of view, the use of this direction can be justified by advocating the damage model proposed back in the 1970s by Kanazawa, Miller and Brown [45] and based on an extensive experimental investigation. In particular, according to their pivotal findings, Stage I cracks in ductile metals subjected to multiaxial fatigue loading always initiate on those crystallographic planes that are most closely aligned with the maximum shear strain direction. In this setting, the direction of maximum variance of the resolved shear strain is then that physical direction experiencing the maximum variation of the shear stress/strain components.
As far as constant amplitude (CA) load histories are concerned, the amplitude (γ_a, τ_a, and $\sigma_{n,a}$) and the mean value (γ_m, τ_m, and $\sigma_{n,m}$) of the stress and strain components relative to the critical plane are determined directly via the following standard definitions (see also Fig. 1c):

$$\gamma_m = \frac{1}{2}\left(\gamma_{MV,max} + \gamma_{MV,min}\right) \tag{1a}$$
$$\gamma_a = \frac{1}{2}\left(\gamma_{MV,max} - \gamma_{MV,min}\right) \tag{1b}$$
$$\tau_m = \frac{1}{2}\left(\tau_{MV,max} + \tau_{MV,min}\right) \tag{2a}$$
$$\tau_a = \frac{1}{2}\left(\tau_{MV,max} - \tau_{MV,min}\right) \tag{2b}$$

$$\sigma_{n,m} = \frac{1}{2}\left(\sigma_{n,max} + \sigma_{n,min}\right) \tag{3a}$$
$$\sigma_{n,a} = \frac{1}{2}\left(\sigma_{n,max} - \sigma_{n,min}\right) \tag{3b}$$

In Eqs (1a) and (1b) $\gamma_{MV,max}$ and $\gamma_{MV,min}$ are the maximum and minimum value of $\gamma_{MV}(t)$, respectively, whereas in Eqs (2a) and (2b) $\tau_{MV,max}$ and $\tau_{MV,min}$ are the maximum and minimum value of the shear stress, $\tau_{MV}(t)$, resolved along direction MV (Figs 1b and 1c). In a similar way, in definitions (3a) and (3b) the amplitude, $\sigma_{n,a}$, and the mean value, $\sigma_{n,m}$, of the stress perpendicular to the critical plane are determined via the maximum, $\sigma_{n,max}$, and minimum, $\sigma_{n,min}$, value of normal stress $\sigma_n(t)$ – see Figs 1b and 1c.
Assume now that the material point of interest in the structural component being designed (Fig. 1a) experiences a stress/strain state whose components vary randomly, with T denoting the time length of the observation period. As soon as the direction, MV, experiencing the maximum variance of the resolved shear strain is known (Fig. 1b), the mean values and the equivalent amplitudes of the shear stress/shear strain components relative to the critical plane take on the following values (Fig. 1d) [43]:

$$\gamma_m = \frac{1}{T}\int_0^T \gamma_{MV}(t) \cdot dt \tag{4a}$$
$$\gamma_a = \sqrt{2 \cdot Var[\gamma_{MV}(t)]} \tag{4b}$$
$$\tau_m = \frac{1}{T}\int_0^T \tau_{MV}(t) \cdot dt \tag{5a}$$
$$\tau_a = \sqrt{2 \cdot Var[\tau_{MV}(t)]} \tag{5b}$$
$$\sigma_{n,m} = \frac{1}{T}\int_0^T \sigma_n(t) \cdot dt \tag{6a}$$
$$\sigma_{n,a} = \sqrt{2 \cdot Var[\sigma_n(t)]} \tag{6b}$$

where the variance terms are calculated as:

$$\begin{aligned} Var[\gamma_{MV}(t)] &= \frac{1}{T}\int_0^T [\gamma_{MV}(t) - \gamma_m]^2 \cdot dt \\ Var[\tau_{MV}(t)] &= \frac{1}{T}\int_0^T [\tau_{MV}(t) - \tau_m]^2 \cdot dt \\ Var[\sigma_n(t)] &= \frac{1}{T}\int_0^T \left[\sigma_n(t) - \sigma_{n,m}\right]^2 \cdot dt \end{aligned} \tag{7}$$

As demonstrated in Refs [42], the first key advantage of using the γ-MVM in situations of practical interest is that this approach allows the time needed to determine the orientation of the critical plane to be reduced markedly. The second key advantage is that the shear stresses and shear strains relative to the critical plane are managed and quantified via resolved quantities $\tau_{MV}(t)$ and $\gamma_{MV}(t)$, respectively. Since, by definition, both $\tau_{MV}(t)$ and $\gamma_{MV}(t)$ are monodimensional stress/strain signals, fatigue cycles under multiaxial fatigue loading can be counted rigorously and effectively by simply using one of those methods that were originally formulated to specifically assess uniaxial fatigue situations (such as, for instance, the well-known Rain-Flow counting method [46, 47]). These two unique features explain the reason why the development of the novel fatigue design methodology being proposed in the present paper is fully based on the γ-MVM.

2.2. The Modified Manson-Coffin Curve Method under constant amplitude loading
The mathematical formulation of the MMCCM takes as a starting point the experimental observation [47, 48] that Stage I cracks initiate on those crystallographic planes that are almost parallel to the direction experiencing the maximum shear strain amplitude. Further, much experimental evidence suggests that the subsequent propagation phase is influenced not only by the amplitude [49], but also by the mean value [48] of the stress perpendicular to the Stage I plane. According to this fatigue damage model, the specific features of the stress state at the assumed crack initiation site can directly be quantified and modelled via critical plane stress ratio ρ which is defined as [2, 41]:

$$\rho = \frac{\sigma_{n,m}+\sigma_{n,a}}{\tau_a} = \frac{\sigma_{n,max}}{\tau_a} \tag{8}$$

In Eq. (8) τ_a is the shear stress amplitude relative to the plane of maximum shear strain amplitude, whilst $\sigma_{n,m}$, $\sigma_{n,a}$ and $\sigma_{n,max}$ are the mean value, the amplitude and the maximum value of the stress perpendicular to the critical plane, respectively. It is worth recalling here that, thanks to the way it is defined, ratio ρ is sensitive not only to the degree of multiaxiality and non-proportionality of the applied loading path, but also to the presence of superimposed static stresses [41, 42].

Fatigue assessment according to the MMCCM is performed via non-conventional bi-parametrical Manson-Coffin curves whose calibration constants change as stress ratio ρ varies [41]. In more detail, according to the schematic γ_a vs. $2N_f$ log-log diagram reported in Fig. 2a, different modified Manson-Coffin curves are obtained as ratio ρ increases, with each of these curves being expressed mathematically via the following relationship:

$$\gamma_a = \frac{\tau'_f(\rho)}{G}\left(2 \cdot N_f\right)^{b(\rho)} + \gamma'_f(\rho) \cdot \left(2 \cdot N_f\right)^{c(\rho)} \tag{9}$$

In Eq. (9) the calibration constants being required are derived directly from the fully-reversed uniaxial (ρ=1) and torsional (ρ=0) Manson-Coffin fatigue curves as follows [2, 41]:

$$\begin{aligned}
\frac{\tau'_f(\rho)}{G} &= \rho \cdot (1+\nu_e)\frac{\sigma'_f}{E} + (1-\rho)\frac{\tau'_f}{G} \\
\gamma'_f(\rho) &= \rho \cdot \left(1+\nu_p\right)\varepsilon'_f + (1-\rho)\gamma'_f \\
b(\rho) &= \frac{b \cdot b_0}{(b_0-b)\rho+b} \\
c(\rho) &= \frac{c \cdot c_0}{(c_0-c)\rho+c}
\end{aligned} \tag{10}$$

where ν_e and ν_p are Poisson's ratio for elastic and plastic strain, respectively, whereas the meaning of the other material constants being used is explained in the Nomenclature.

According to Fig. 2a as well as to Eq. (9), for a given material, the corresponding modified Manson-Coffin curves are seen to move downwards as ratio ρ increases [2, 41]. This means that the MMCCM performs the fatigue assessment based on the hypothesis that, for a given value of γ_a, the extent of fatigue damage increases as ratio ρ increases.

An important aspect that must be considered here in detail is that calibration constants (10) can be used to estimate the position of the necessary modified Manson-Coffin curve as long as ratio ρ is lower than a specific threshold value (denoted as ρ_{lim}), with this limit ratio being determined by running appropriate experiments. In contrast, when the experimental value of ρ is larger than ρ_{lim}, the constants of the modified Manson-Coffin curve to be used to estimate fatigue life time are recommended to be derived still from calibration functions (10), but by setting ρ invariably equal to ρ_{lim}. This correction is suggested to be used to model (in an simplified way) the fact that in the presence of large values of stress ratio ρ, fatigue damage is no longer governed solely by the shearing forces [2]. This is the reason why, when $\sigma_{n,max}$ is much larger than τ_a, the classic critical plane approach is seen to return predictions that are characterised by a very large level of conservatism [13, 50, 51]. This can be seen as a consequence of the fact that, as soon as $\sigma_{n,m}$ becomes larger than a material-dependant threshold value, a further increase of the mean stress perpendicular to the critical plane does not lead to a further increase of the resulting fatigue damage [48, 50]. This experimental evidence was explained by Kaufman and Toper [48] by observing that, when $\sigma_{n,m}$ is lower than the aforementioned material threshold, the magnitude of the shearing forces guiding the crack growth process is reduced due to the friction between the two surfaces of the Stage I crack itself. This friction clearly reduces the crack propagation rate markedly. In contrast, when $\sigma_{n,m}$ is larger than this material threshold, the shearing forces are fully transmitted to the tips of the cracks, with this favouring the propagation process. This situation results in the fact that, when

micro/meso cracks are fully open, a further increment of the mean stress perpendicular to the Stage I plane does not lead to a further increment of the crack propagation rate [48]. As mentioned above, these phenomena are incorporated into the MMCCM by simply assuming that, when ρ is larger than ρ_{lim}, the constants in Eq. (9) are estimated from calibration functions (10) by setting ρ invariably equal to ρ_{lim}.
To conclude, it is worth recalling here that, under time-variable loading, there are always at least two material planes on which the shear strain amplitude reaches its maximum value. Therefore, when choosing the critical plane amongst those planes experiencing the maximum shear strain amplitude, the plane that must be used to estimate the extent of fatigue damage according to the MMCCM is the one which is associated with the largest value of stress ratio ρ [41, 42].

2.3. The elasto-plastic Theory of Critical Distances

The core idea on which the TCD is based was first proposed by Neuber [4] and Peterson [5] in the 1940s-50s to specifically address the high-cycle notch fatigue problem. The common feature of the different formalisations of the TCD is that the extent of damage is quantified via a design quantity that depends not only on the magnitude of the local stress/strain fields acting on the material in the vicinity of the crack initiation locations, but also on a material length scale parameter, L [10, 32]. In the TCD framework the critical distance, L, is treated as a material constant which is independent from the geometrical features of the stress concentrator being assessed [10].
The TCD can be formalised in different ways which include the Point, Line, Area and Volume Method [10]. In more detail, the Volume Method (VM) assumes that the design quantity to be used to estimate fatigue strength has to be calculated by averaging the stresses/strains over a reference material volume in the vicinity of the notch being assessed [10]. According to the Area Method (AM), the same design quantity can also be determined by simply averaging the local stresses/strains over a reference area having size of the order of L. The VM and AM's *modus operandi* suggests that the TCD assesses fatigue strength of notched/cracked materials by post-processing the entire stress/strain fields acting on a process zone whose size mainly depends on the material microstructural features as well as on the local micro-mechanical properties (Fig. 2b) [2, 10, 32]. This process zone represents the portion of material that controls the overall fatigue strength of the component being assessed and, according to both the VM and AM, its size approaches L (Fig. 2b) [2, 10].
Unfortunately, using the VM and AM in situations of practical interest is not at all straightforward because averaging stress/strain fields in 2D/3D domains is never a trivial task. However, the problem can be simplified greatly by observing that, as postulated by the Line Method (LM), the design quantity of interest can be determined also by averaging the relevant stress/strain components along a line having length equal to 2L. Finally, a further simplification can be introduced by applying the TCD in the form of the Point Method (PM). The PM postulates that the design quantity of interest can directly be taken equal to the stress/strain relative to a point that is positioned at a distance from the crack/notch tip equal to L/2 - i.e., at the centre of the process zone (Fig. 2b) [10, 32].
Taking as a starting point the unique features of the TCD, recently an elasto-plastic reformulation of this theory was proposed to estimate lifetime of notched metallic materials experiencing cyclic plastic deformations in the crack initiation regions [32, 33]. This problem was addressed by defining the TCD design quantity being used not only according to the classic approach due to Manson and Coffin [19, 20], but also according to the solutions proposed by Smith, Watson and Topper [22] as well as by Morrow [21, 52]. The accuracy and reliability of this alternative formulation of the TCD was checked by using a large number of experimental data we generated by testing, under both CA [32] and VA [33] uniaxial load histories, notched specimens made from different ferrous and non-ferrous metallic materials. The sound agreement we obtained between experimental and estimated fatigue lifetime prompted us to extend the use of the elasto-plastic TCD to those notch situations involving multiaxial fatigue loading. The key feature of the new approach being proposed here are explained in the next section.

3. Formulation of the novel fatigue lifetime estimation methodology

The multiaxial fatigue life estimation methodology being formulated and validated in the present paper makes use of the three tools reviewed in Section 2, i.e., the MMCCM, the γ-MVM, and the elasto-plastic

TCD (applied in the form of the PM). The key features of the novel design approach being proposed will be explained in Section 3.1 and in Section 3.2 by considering CA loading paths and VA load histories, respectively. It is important to point out here that, for the sake of clarity, in these two Sections our novel multiaxial fatigue assessment methodology will be formulated by assuming that the required critical distance, L, is known *a priori*. The procedure being recommended for the experimental determination of critical distance L will be explained in detail in Section 3.3.

3.1. Constant amplitude solution

Figure 3 summarises the design methodology we have devised to estimate CA fatigue lifetime of notched components by applying the MMCCM along with the elasto-plastic PM. Consider then the notched body sketched in Figure 3a and assume that, during in-service operations, this structural detail is subjected to a complex system of time-variable external forces and moments.

To use the MMCCM in conjunction with the PM effectively, the first task to be completed is the determination of the elasto-plastic cyclic stress/strain fields along the so-called focus path. In this context, the focus path is defined as a straight line that originates from the assumed crack initiation point (i.e., point A in Figure 3a) and is normal to the component surface at the hot spot itself (Fig. 3a) [2, 39]. This rule to determine the orientation of the focus path was devised by making the most of the process zone concept [2, 4, 11]. In particular, as per the reasoning summarised in Section 2.1, initiation and early growth of Stage I cracks is assumed to be governed by the micro-stress/strain components acting on those slip planes that are most closely aligned with the macroscopic material planes of maximum shear [45]. Owing to the fact that, in practice, the orientation of the above crystallographic planes is never known, by taking full advantage of the VM [10], a macroscopic stress/strain state that is representative of the extent of damage associated with those grains in the vicinity of the assumed crack initiation location can be estimated by simply averaging the stress/strain fields over the process zone itself (Fig. 2b). Since the effective stress/strain state estimated in terms of the VM is the same as the one that is calculated according to the PM [10], the problem can greatly be simplified by simply using the time-variable stress/strain tensors estimated at the centre of the process zone (Fig. 2b). This fairly articulated reasoning leads to the conclusion that the stress/strain state estimated at the centre of the process zone can be seen as an engineering quantity which is representative of the microscopic stress/strain state damaging those grains in the vicinity of the crack initiation site [2]. In this setting, the assumption can be made that the shear/normal macroscopic stress/strain components relative to the plane of maximum shear are proportional to the corresponding microscopic stress/strain quantities acting on the most damaged easy glide planes [2, 11]. Accordingly, the centre of the process zone becomes the reference material point to be used to estimate the stress/strain tensors needed to perform the fatigue assessment. By so doing, the obvious hypothesis which can be formed to define the focus path is that this path is a straight line emanating from the crack initiation point and normal to the component surface at the crack initiation point itself – i.e., according to Fig. 3a, the focus path originates from point A and passes through the centre of the process zone. The validity of this simple geometrical rule suitable for defining the orientation of the focus path has been demonstrated in a number of technical articles published in the recent past [11, 12, 13, 37, 39].

Having defined the orientation of the focus path, as per the PM's *modus operandi*, the relevant stress/strain quantities needed to estimate fatigue lifetime have to be determined by post-processing the cyclic stress tensor, $[\sigma(t)]$, and the cyclic stain tensor, $[\varepsilon(t)]$, evaluated, along the focus path, at a distance from the assumed crack initiation point equal to L/2 (i.e., at point O in Figure 3a).

The direction of maximum variance of the resolved shear strain and, therefore, the orientation of the critical plane are then determined from the time-variable strain tensor, $[\varepsilon(t)]$, at point O by making use of the γ-MVM (Section 2.1). As soon as the direction, MV, of maximum variance of the resolved shear strain is known (Fig. 3b), both the maximum shear strain amplitude γ_a (Fig. 3c) and the maximum shear stress amplitude τ_a (Fig. 3d) can directly be determined according to definition (1b) and definition (2b), respectively. In a similar way, by post-processing stress signal $\sigma_n(t)$, the mean value and the amplitude of the stress perpendicular to the critical plane can be calculated unambiguously by using Eq. (3a) and Eq. (3b), respectively (Fig. 3e).

The values for τ_a, $\sigma_{n,m}$, and $\sigma_{n,a}$ being determined via the γ-MVM are then used to quantify through definition (8) the stress ratio relative to the critical plane, ρ (Fig. 3f). According to the calculated value for ratio ρ, the corresponding modified Manson-Coffin curve, Eq. (9), is then estimated directly via calibration functions (10) – see Fig. 3g. Finally, as shown in the Modified Manson-Coffin diagram sketched in Figure 3h, the modified Manson-Coffin curve being estimated via Eq. (9) allows the number of reversals to failure, $2N_f$, to be estimated directly.

3.2. Variable amplitude solution

The methodology we devised to use the MMCCM in conjunction with the elasto-plastic PM to address the VA multiaxial notch fatigue problem is summarised in Figure 4.

Consider the notched component of Figure 4a and assume that this structural detail is subjected to a complex system of external time-variable forces and moments. This load history is hypothesised to result in local VA multiaxial stress/strain fields acting on the material in the vicinity of the notch being designed.

As per the CA case, under VA loading as well the first problem to be addressed is the determination of the elasto-plastic cyclic stress/strain distributions along the focus path. As soon as the relevant stress/strain fields are known, the required tensors (i.e., $[\sigma(t)]$ and $[\varepsilon(t)]$) are determined at a distance from the assumed crack initiation point equal to L/2 (Fig. 1a). Subsequently, tensor $[\varepsilon(t)]$ is post-processed by making use of the γ-MVM so that the direction, MV, experiencing the maximum variance of the resolved shear strain is determined unambiguously (Fig. 4b).

After determining the orientation of direction MV (Fig. 4b), the equivalent amplitude of the shear stress acting on the critical plane, τ_a, is calculated via Eq. (5b) – see Fig. 4c. In a similar way, the mean value, $\sigma_{n,m}$, and the equivalent amplitude, $\sigma_{n,a}$, of the stress perpendicular to the critical plane are determined via definition (6a) and definition (6b), respectively (Fig. 4d). Equivalent stress components τ_a and $\sigma_{n,max}$ (where $\sigma_{n,max}=\sigma_{n,m}+\sigma_{n,a}$) are then used along with definition (8) to determine the value of the critical plane stress ratio, ρ, characterising the VA fatigue load history being assessed (Fig. 4e). By so doing, ratio ρ and functions (10) allow the constants in the MMCCM to be estimated directly (Fig. 4f).

After deriving the modified Manson-Coffin curve needed to assess fatigue damage (Fig. 4g), the next step is using the Rain-Flow cycle counting method [46, 47] to post-process monodimensional signal $\gamma_{MV}(t)$ so that the shear strain spectrum associated with the load history being assessed is determined unambiguously (Figs 4h and 4i). This shear strain spectrum (Fig. 4j) and the modified Manson-Coffin curve estimated via Eq. (9) are then employed to quantify the damage associated with any shear strain cycles being counted (Fig. 4g). Finally, the number of cycles to failure can directly be predicted as follows (Fig. 4k):

$$D_{tot} = \sum_{i=1}^{j} \frac{n_i}{N_{f,i}} \Rightarrow N_{f,e} = \frac{D_{cr}}{D_{tot}} \sum_{i=1}^{j} n_i \tag{11}$$

In the above relationships, D_{tot} is the total value of the damage sum, whereas D_{cr} is the critical value of D_{tot} resulting in the initiation of a fatigue crack in the notched component being assessed.

To conclude, it is important to point out that the classic theory as devised by Palmgren [53] and Miner [54] postulates that D_{cr} should be invariably equal to unity. However, in situations of practical interest the value of the critical damage sum is seen to vary in range 0.02-5, where the only way to determine D_{cr} accurately is by running appropriate experiments [55].

3.3. Experimental determination of the critical distance

The formulation of the multiaxial notch fatigue design methodology summarised in the previous sub-sections takes as a starting point the assumption that critical distance L is known *a priori*, with length L being a material property to be determined by running appropriate experiments.

Figure 2c summarises the procedure we recommend for the experimental determination of L. To this end, the uniaxial and torsional fatigue properties of the plain (i.e., un-notched) material under investigation are supposed to be known. This means that calibration constants in the MMCCM – i.e., Eqs (10) - can be determined accurately as critical plane ratio ρ varies.

Consider now the notched specimen of Fig. 2c and assume that this sample is subjected to a fully-reversed nominal uniaxial loading. Under the applied CA loading path, this sample is seen to fail at a number of cycles to failure equal to $N_{f,c}$.
The stress/strain-distance curves along the focus path associated with the investigated notched geometry are to be determined by directly post-processing the results from an elasto-plastic Finite Element (FE) model. Subsequently, the stress and strain components along the focus path are post-processed according to the γ-MVM. By so doing, the distribution of γ_a, τ_a, $\sigma_{n,max}$, and ρ along the focus path itself can be determined unambiguously (Fig. 2c). Finally, according to the PM, L/2 is the distance from the notch tip at which the shear strain amplitude, γ_a^*, is equal to the shear strain amplitude estimated from the MMCCM, Eq. (9), that causes failure in the plain material at $N_f=N_{f,c}$ (Fig. 2c).
Turning to the type of geometrical feature to be used to estimate length L, according to our previous experience [32, 33], the usage of notches that are as sharp as possible is advisable. This is because the TCD should always be calibrated by considering the two extreme cases, i.e., plain and cracked material. Since metallic materials' fatigue behaviour in the presence of very sharp stress raisers is seen to be similar to that observed in the presence of cracks [10], critical length L is then recommended to be estimated by testing notches with tip radius as small as possible.
To conclude, it is important to highlight that, in theory, only one single calibration test would be enough to estimate L. However, due to the inevitable scattering that always characterises fatigue data, the use of several calibration tests is always recommended.

4. Experimental details, material fatigue properties and cracking behaviour

To check the accuracy and reliability of the multiaxial notch fatigue design methodology formulated in Section 2, a systematic experimental investigation was carried out by testing the plain and V-notched cylindrical specimens that are sketched in Fig. 5a. As far as the notched samples are concerned, this figure also shows the values of the net stress concentration factors, where K_t and K_{tt} were estimated under tension and torsion, respectively, by using *ad hoc* analytical solutions [56, 57].
The material being tested was unalloyed medium-carbon steel En8 (080M40) that had ultimate tensile stress, σ_{UTS}, equal to 701 MPa, yield stress, σ_Y, to 453 MPa, and Young's modulus, E, to 210 GPa.
The experimental results needed to check the accuracy of our novel design approach were generated by using a SCHENCK servo-controlled closed-loop axial-torsion fatigue machine with maximum axial load capacity of 400 kN and maximum torque capacity of 1000 Nm. The cylindrical specimens were clamped using two MTS 646.25S hydraulic collet grips.
The strain-controlled tests as well as the force/torque-controlled tests were run under CA/VA sinusoidal loading signals, with the frequency varying in the range 0.5-2 Hz. The experimental results obtained by testing the un-notched specimens were generated by controlling the axial and the shear strains via an Epsilon 3550-025M bi-axial extensometer with gauge length equal to 25 mm.
Fatigue failures (i.e., the number of cycles/blocks to failure) were defined both for the plain specimens and the notched samples by 5% axial/torsional stiffness drop, with the stiffness decrease being estimated under the maximum amplitude of the strain/force applied in the loading path. To observe and analyse the cracking behaviour displayed by the investigated material both in the presence and in the absence of stress/strain concentration phenomena, all the tests were run up to the complete breakage of the specimens.
By adopting the concave upwards spectrum with sequence length, S_L, of 50 cycles that is shown in Fig. 5b, the VA fatigue behaviour of the plain and notched specimens of Fig. 5a was investigated by controlling the axial/shear strain and the axial/torsional loading, respectively. In the spectrum of Fig. 5b, given either the axial force, the torque, the axial strain, or the shear strain, $\Omega_{a,i}$ denotes the amplitude of the reference strain/loading quantity characterising the i-th cycles, whereas $\Omega_{a,max}$ denotes the maximum value in the spectrum of the amplitude of the strain/loading quantity of interest. As to the results generated under VA loading, it is important to point out here that all the cycles were applied in random order (Fig. 5c), with the instantaneous values of the strain/load channels being gathered during testing systematically.
The cyclic mechanical properties of the steel being investigated were determined by testing the plain cylindrical samples under fully-reversed axial strain as well as under fully-reversed shear strain (Tab.

1). These results were then post-processed to determine the axial (Fig. 5d) and torsional (Fig. 5e) stabilised stress-strain curves as well as the uniaxial (Fig. 5f) and torsional (Fig. 5g) Manson-Coffin curves. All the strain-controlled testes being run are summarised in Tab. 1, with this table listing not only the results obtained under pure uniaxial and pure torsional fatigue loading, but also those generated under CA and VA axial/torsion load histories. In Tab. 1, symbols $\varepsilon_{x,a\text{-}max}$ and $\gamma_{xy,a\text{-}max}$ are used to denote the maximum value of the amplitude during testing. Clearly, under CA fatigue loading, $\varepsilon_{x,a\text{-}max}$ and $\gamma_{xy,a\text{-}max}$ were equal to the amplitude of the constant amplitude sinusoidal strain signal that was applied to the plain specimens being tested.
All the force/torque-controlled experimental results we generated by testing the notched specimens are listed in Tables 2 to 5. In these tables, the tests we ran are described in terms of: maximum amplitude in the load history (either CA or VA) of the axial, $F_{a\text{-}max}$, and torsional, $T_{a\text{-}max}$, loading; load ratio, R; out-of-phase angle, δ; ratio f between the frequencies of the two loading channels; and, finally, experimental value of the number of cycles to failure, N_f (or number of blocks to failure, N_b).
Turning to the cracking behaviour that was observed in the plain specimens, the crack initiation process was seen to occur always on those material planes experiencing the maximum shear stress/strain amplitude, with this holding true independently of the complexity of the loading path being applied. This conventional Mode II governed initiation process (Stage I) can be seen clearly in the pictures reported in Figs 6a and 6b. In particular, under uniaxial fatigue loading, the crack initiation process as well as the initial propagation phase were seen to occur always on materials planes that were at 45° to the specimen's axis (Fig. 6a). In contrast, under pure torsional loading, the cracks were seen to initiate and propagate along material planes that were either parallel or perpendicular to the longitudinal axis of the samples (Fig. 6b).
The failure matrix reported in Fig. 6d provides an overview of the fracture surfaces that were observed in the notched specimens tested under both CA and VA load history. According not only to the failure matrix of Fig. 6d, but also to the picture reported in Fig. 6c, in the notched specimens cracks initiated, at the notch roots, always on those planes of maximum shear stress/strain amplitude (i.e., Stage I cracks whose initiation was Mode II governed). Subsequently, these notch tip circumferential cracks were seen to radially propagate toward the centre of the net cross-sectional area. After exhausting the initial Stage I phase, the branching phenomenon occurred and cracks kept growing by changing their orientation so that they could experience the maximum Mode I loading (Stage II process). This complex cracking process was seen to result always in the formation of "factory roof" failure surfaces (Figs 6c and 6d).
The massive body of experimental work summarised in Tables 1 to 5 will be used in what follows to calibrate the fatigue design approach devised in Section 2 as well as to check its accuracy and reliability in estimating the lifetime of the notched specimens we tested under CA and VA multiaxial fatigue loading.

5. Numerical stress/strain analyses

One of the key features of the fatigue design methodology being formulated in Section 2 is that the extent of damage can be estimated provided that the elasto-plastic cyclic stress/strain fields in the vicinity of the tip of the notches being assessed are known. Since the available analytical solutions [25-28] are suitable for estimating stresses and strains solely at the notch tip, the only way to determine the required stress/strain fields is by solving cyclic elasto-plastic FE models. In this context, being able to reach an adequate level of accuracy implies using numerical techniques capable of accurately quantifying/modelling important phenomena that include, amongst other, strain hardening/softening, non-proportional hardening, ratcheting, memory effect, and mean stress relaxation.
Owing to the fact that sub-surface stress/strain fields in notched metallic materials subjected to fatigue loading cannot be determined experimentally, the only way to build up the necessary confidence in the FE code being used is by modelling the elasto-plastic mechanical response of un-notched materials. This is a useful exercise because, in plain metals, the superficial stresses and strains can not only be quantified experimentally, but also estimated analytically by using very accurate tools - such as, for instance, the well-known approach devised by Jiang and Sehitoglu [58, 59].
In the present investigation local elasto-plastic cyclic stresses and strains were modelled numerically by using commercial FE code ANSYS®. According to the strategy mentioned above, we built up our

confidence in this software by checking its accuracy in modelling/estimating the elsto-plastic stresses and strains on the surface not only of the plain specimens we tested under strain control (Tab. 1), but also of a number of un-notched tubular specimens made of different metallic materials (Tab. 6). The results obtained by testing plain tubular samples were taken from the technical literature and they were generated by considering a variety of CA and VA axial/torsional loading paths. Some of the load histories that were post-processed to implement the present validation exercise are shown in Fig. 7.

The tubular (Fig. 8a) and cylindrical (Fig. 8b) specimens employed for this initial validation exercise were modelled in ANSYS® using three-dimensional 8-node structural element SOLID185. A multi-linear kinematic rule was adopted to model the cyclic elasto-plastic behaviour of the considered metallic materials, with the mechanical response being quantified solely via the axial stabilised stress-strain curve. In the different FE models being solved, the mesh density was gradually increased until convergence occurred in terms of linear-elastic stresses. To model the results generated under CA loading, six complete virtual cycles were run for any loading path being analysed. This was done to allow the numerical solution to reach a stabilised configuration for the stress vs. strain response. Under VA loading instead, local elasto-plastic stresses and strains were determined by simulating two loading blocks. It is important to point out here also that all the numerical simulations were run by using as boundary conditions the considered load histories expressed in terms of axial displacements and torsional rotation angles. In other words, the simulations were run by assuming that the considered CA and VA loading histories were known in terms of strains, with the corresponding elasto-plastic stresses being estimated both numerically and analytically.

As far as the results taken from the technical literature are concerned, the stress vs. strain graphs of Fig. 9 show (as an example) seven sets of hysteresis loops from the twenty different numerical simulations that we ran using FE code ANSYS®. These charts also compare the hysteresis loops obtained experimentally to the corresponding ones estimated via Jiang and Sehitoglu's analytical method [58, 59].

The diagrams reported in Fig. 10 summarise instead the accuracy of ANSYS® in modelling the stress vs. strain response of the plain cylindrical specimens we tested under both CA and VA loading (see also Tab. 1). The charts of Fig. 10 make it evident that, as far as the carbon steel being tested was concerned, ANSYS® was capable of estimating the maximum values of the stresses in the cycles with a remarkable level of accuracy, the maximum error in terms of stress amplitude being of the order of 15%. In contrast, the areas of the estimated hysteresis loops were seen to be systematically larger than the corresponding areas of the experimental stress vs. strain loops.

This validation exercise allowed us to come to two relevant conclusions. First, commercial FE code ANSYS® is capable of modelling the elasto-plastic stress vs. strain response of metallic materials by reaching the same level of accuracy as the one that is obtained by using the well-known analytical solution devised by Jiang and Sehitoglu [58, 59] (Fig. 9). Second, when the cyclic elasto-plastic mechanical properties of the parent material are known from the experiments, both the numerical and the analytical solutions are capable of estimating the maximum values of the stress components in the CA and VA cycles well within an error factor of two (Figs 9 and 10a).

To conclude the present section, it has to be pointed out that both the numerical and the analytical approach being used were seen to result always in a certain level of inaccuracy in estimating the maximum values of the cyclic stress components. This is a very important aspect because, clearly, the error that is made in the stress/strain analysis phase propagates itself by ending up affecting also the overall accuracy that is obtained when estimating fatigue lifetime. However, since the error associated with the stress/strain analyses cannot be eliminated, this intrinsic limitation must be borne in mind when using estimated values for the elasto-plastic stresses and strains to perform fatigue assessment in situations of practical interest.

6. Validation by experimental data

In order to check the overall accuracy of the design methodology being formulated in Section 3, the first step was calibrating the MMCCM's governing relationships, i.e. Eqs (10). This was done by directly using the values of the parent material fatigue constants that we determined by testing the plain specimens both under fully-reversed uniaxial loading and under fully-reversed torsional loading (see Figs 5d to 5g).

Subsequently, attention was focussed on the estimation of the limit value of critical plane stress ratio, ρ_{lim}. To this end, we used the experimental result that we generated by testing an un-notched specimen under 90° out-of-phase CA axial loading and torsion with non-zero mean strain (i.e., test PSBCANZMSOoPh2 in Tab. 1). This experimental datum was chosen because this complex CA loading path resulted in a large value of ρ, i.e. ρ=2.2, so that it could be used to directly solve Eq. (9) for ρ_{lim}, i.e.:

$$\gamma_a = \frac{\tau'_f(\rho_{lim})}{G}\left(2 \cdot N_f\right)^{b(\rho_{lim})} + \gamma'_f(\rho_{lim}) \cdot \left(2 \cdot N_f\right)^{c(\rho_{lim})} \Rightarrow \rho_{lim} = 1.7,$$

where the amplitude of the shear strain relative to the critical plane, γ_a, was calculated to be 0.0039, with the experimental number of cycles to failure, N_f, being equal to 1356 (see also Tab. 1).
Having calibrated the MMCCM for the specific carbon steel being tested, the subsequent step was checking the accuracy of our multiaxial fatigue criterion in estimating fatigue lifetime in the absence of stress/strain concentration phenomena. To this end, the results generated under CA and VA biaxial loading that are listed in Tab. 1 were post-processed to determine the stress/strain quantities relative to the critical plane that were needed to estimate lifetime according to Eq. (9) [41, 42].
The experimental, N_f, vs. estimated, $N_{f,e}$, number of cycles to failure diagram reported in Fig. 11a summarises the overall accuracy that was obtained by applying the MMCCM to post-process the data listed in Tab. 1. According to Palmgren [53] and Miner [54], the predictions under VA loading shown in Fig. 11a were obtained by taking the critical value of the damage sum, D_{cr}, invariably equal to unity. This error chart demonstrates that the use of our critical plane approach resulted in estimates falling within an error factor of 2, i.e., within a scatter band as wide as the one containing the fatigue results generated under axial and torsional CA fatigue loading and used to calibrate the MMCCM itself. This suggests that the level of accuracy obtained is as good as possible, since we cannot ask a predictive method to be, from a statistical point of view, more accurate than the experimental information used to calibrate the method itself. Accordingly, this level of error will be used in what follows to assess the overall accuracy of our novel design methodology in estimating lifetime of notched components subjected to CA/VA multiaxial fatigue loading.
In order to post-process the experimental results we generated by testing the notched specimens (Tabs 2 to 5) to check the accuracy of our novel design methodology, commercial FE code ANSYS® was used to determine the required time-variable elasto-plastic stress/strain fields. In particular, the notched specimens of Fig. 5a were modelled using three-dimensional 8-node structural element SOLID185. The elasto-plastic behaviour of the tested carbon steel was simulated by adopting a multi-linear kinematic rule that was calibrated via the axial stabilised stress-strain curve experimentally generated by testing the plain specimens (Fig. 5d). Very refined mesh was used to model the material in the vicinity of the tips of the notches being investigated (Figs 8c, 8d, and 8e). Convergence in the three-dimensional FE models was tested by comparing the linear-elastic stress fields being determined under pure tension as well as under pure torsion to the corresponding ones calculated by using simple axisymmetric bi-dimensional elements. Stress-strain elasto-plastic numerical analyses were run by simulating six complete virtual cycles and two loading blocks under CA and VA fatigue loading, respectively.
The critical distance value was determined by applying the PM along with the MMCCM as schematically shown in Fig. 2c. In particular, the PM critical distance, L/2, was determined by post-processing the experimental results we generated by testing six sharply notched specimens under uniaxial fatigue loading (see Tab. 2). The critical lengths we calculated were remarkably consistent, with the experimental procedure summarised in Fig. 2c returning values for L/2 varying in the range 0.76 mm-0.80 mm. Such a high level of consistency fully supports the idea that the elasto-plastic TCD [32, 33] can successfully be applied also along with suitable multiaxial fatigue criteria.
According to the critical lengths being estimated, an average value for L/2 of 0.78 mm was then used for the final validation exercise, whose results are summarised in the error diagrams of Figs 11b to 11e. In more detail, these charts of Figs 11b, 11c, and 11d were built by plotting the experimental, N_f, against the estimated, $N_{f,e}$, number of cycles to failure for the different CA and VA load history being considered. The error diagram of Fig. 11e summarises instead the accuracy in terms of number of blocks to failure of our approach in estimating fatigue lifetime when the axial and torsional loading were applied at

different frequencies. As per the un-notched samples, also the VA fatigue lifetime of the notched specimens was determined, as recommended by Palmgren [53] and Miner [54], by setting the critical value of the damage sum, D_{cr}, invariably equal to unity. These charts make it evident that the use of our multiaxial fatigue life estimation technique resulted in a very high level of accuracy, with all the experimental results falling within an error factor of 2. Such a degree of precision is clearly very satisfactory especially because these estimates were obtained by post-processing results generated by testing notches of different sharpness under very complex CA and VA loading paths, with these load histories involving different levels of non-proportionality, non-zero mean stresses, and axial/torsional load signals applied at different frequencies.
To conclude, it can be said that, when the stress/strain analysis is performed by explicitly modelling the elasto-plastic cyclic behaviour of metallic materials, the design approach formulated and validated in the present paper offers to date the most complete solution to the multiaxial notch fatigue problem.

7. Conclusions

In the present paper a novel multiaxial notch fatigue life estimation technique based on the combined use of the MMCCM, the γ-MVM, and the elasto-plastic PM is formulated first and the validated against a large number of experimental results. The most important conclusions can be summarised as follows:

- the proposed design approach allows notched structural components to be designed against multiaxial fatigue loading by directly post-processing the relevant stress/strain fields determined by solving elasto-plastic FE models;
- the proposed multiaxial fatigue assessment methodology is seen to be successful in estimating the lifetime of notched metallic materials subjected to both CA and VA load histories, with this holding true independently of the sharpness of the notch being designed;
- the use of the design approach being proposed is seen to result in a remarkable level of accuracy also in the presence of load histories involving different levels of non-proportionality, non-zero mean stresses, and load signals applied at different frequencies;
- according to the systematic validation exercise being performed, the use of our novel fatigue design methodology is seen to result in estimates falling within an error factor of 2 (i.e., within a scatter band which is as wide as the one containing the fatigue results generated by testing the plain specimens under axial and torsional CA fatigue loading and used to calibrate the MMCCM);
- more work needs to be done in this area to develop novel technological/numerical solutions that allow the computational time needed to perform the required elasto-plastic stress/strain analyses to be reduced markedly.

Acknowledgements

Support for this PhD research work from the Higher Committee for Education Development in Iraq (HCED) is gratefully acknowledged.

References

[1] R.I. Stephens, A. Fatemi, R.R. Stephens, H.O. Fuchs, Metal Fatigue in Engineering, 2nd Edition, John Wiley & Sons, USA, 2001.
[2] L. Susmel, Multiaxial Notch Fatigue: from nominal to local stress-strain quantities. Woodhead & CRC, Cambridge, UK, 2009.
[3] D.F. Socie, G.B. Marquis, Multiaxial Fatigue, SAE, Warrendale, PA, 2000.
[4] H. Neuber, Theory of notch stresses: principles for exact calculation of strength with reference to structural form and material, 2nd Edition, Springer-Verlag, Berlin, Germany, 1958.
[5] R.E. Peterson, Notch Sensitivity. In: Metal Fatigue, Edited by G. Sines and J. L. Waisman, McGraw Hill, New York, USA, pp. 293–306, 1959.
[6] H.J. Gough, Engineering Steels under Combined Cyclic and Static stresses. Proc. Inst. Mech. Eng. 160 (1949) 417-440.

[7] S.M. Tipton, D.V. Nelson, Advances in multiaxial fatigue life prediction for components with stress concentrators. Int. J. Fatigue 19 (1997) 503-515.
[8] L. Susmel, P. Lazzarin, A Bi-Parametric Modified Wöhler Curve for High Cycle Multiaxial Fatigue Assessment. Fatigue Fract. Eng. Mater. Struct. 25 (2002) 63-78.
[9] P. Lazzarin, L. Susmel, A Stress-Based Method to Predict Lifetime under Multiaxial Fatigue Loadings. Fatigue Fract. Eng. Mater. Struct. 26 (2003) 1171-1187.
[10] D. Taylor, The Theory of Critical Distances: A new perspective in fracture mechanics. Elsevier, Oxford, UK, 2007.
[11] L. Susmel, A unifying approach to estimate the high-cycle fatigue strength of notched components subjected to both uniaxial and multiaxial cyclic loadings. Fatigue Fract. Eng. Mater. Struct. 27 (2004) 391-411.
[12] L. Susmel, D. Taylor, The Modified Wöhler Curve Method applied along with the Theory of Critical Distances to estimate finite life of notched components subjected to complex multiaxial loading paths. Fatigue Fract. Eng. Mater. Struct. 31 (2008) 1047-1064.
[13] L. Susmel, Multiaxial Fatigue Limits and Material Sensitivity to Non-Zero Mean Stresses Normal to the Critical Planes. Fatigue Fract. Eng. Mater. Struct. 31 (2008) 295-309.
[14] A. Carpinteri, A. Spagnoli, S. Vantadori, C. Bagni, Structural integrity assessment of metallic components undermultiaxial fatigue: the C–S criterion and its evolution. Fatigue Fract. Eng. Mater. Struct. 36 (2013) 870-883.
[15] B. Atzori, F. Berto, P. Lazzarin, M. Quaresimin, Multi-axial fatigue behaviour of a severely notched carbon steel. Int. J. Fatigue 28 (2006) 485-493.
[16] F. Berto, P. Lazzarin, J.R. Yates, Multiaxial fatigue of V-notched steel specimens: a non-conventional application of the local energy method. Fatigue Fract. Eng. Mater. Struct. 34 (2011) 921-943.
[17] R. Branco, J. D. Costa, F. Berto, F. V. Antunes, Fatigue life assessment of notched round bars under multiaxial loading based on the total strain energy density approach. Theor. Appl. Fract. Mec. 97 (2018) 340-348.
[18] G. Meneghetti, A. Campagnolo, F. Berto, K. Tanaka, Notched Ti-6Al-4V titanium bars under multiaxial fatigue: Synthesis of crack initiation life based on the averaged strain energy density. Theor. Appl. Fract. Mec. 96 (2018) 509-533.
[19] S.S. Manson, Behaviour of materials under conditions of thermal stress. National Advisory Committee for Aeronautics, NACA TN-2933, 1954.
[20] L.F. Coffin, A study of the effects of cyclic thermal stresses on a ductile metal. Trans. ASME 76 (1954) 931-950.
[21] J.D. Morrow, Cyclic plastic strain energy and the fatigue of metals. In: Internal friction, damping and cyclic plasticity, ASTM STP 378, Philadelphia, USA, pp. 45-87, 1965.
[22] K.N. Smith, P. Watson, T.H. Topper, A Stress-Strain Function for the Fatigue of Metal. J. Mater. 5 (1970) 767–778.
[23] H. Neuber, Theory of stress concentration for shear-strained prismatical bodies with arbitrary nonlinear stress-strain law, ASME J. Appl. Mech. 28 (1961) 544–550.
[24] G. Glinka, Energy density approach to calculation of inelastic strain-stress near notches and cracks. Eng. Fract. Mech. 22 (1985) 485–508.
[25] M. Hoffmann, T. Seeger, A generalised method for estimating multiaxial elastic-plastic notch stresses and strains. Part 1: Theory. Trans. ASME, J. Eng. Mater. Technol. 107 (1985) 250-254.
[26] M. Hoffmann, T. Seeger, A generalised method for estimating multiaxial elastic-plastic notch stresses and strains. Part 2: Application and general discussion. Trans. ASME, J. Eng. Mater. Technol. 107 (1985) 255-260.
[27] V.B. Köttingen, M.E. Barkey, D.F. Socie, Pseudo stress and pseudo strain based approaches to multiaxial notch analysis. Fatigue Fract. Eng. Mater. Struct. 18 (1995) 981-1006.
[28] A. Ince, G. Glinka, Innovative computational modelling of multiaxial fatigue analysis for notched components. Int. J. Fatigue 82 (2016) 134-145.

[29] S.M. Tipton, J.W. Fash, Multiaxial fatigue life prediction for the SAE specimen using strain based approaches. In: Multiaxial fatigue: analysis and experiments, Edited by G. E. Leese and D. F. Socie, SAE AE-14, pp. 67-80, 1989.
[30] L. Susmel, G. Meneghetti, B. Atzori, A novel Multiaxial Fatigue Criterion to predict Lifetime in the Low/Medium-Cycle Fatigue Regime. Part II: Notches. Trans. ASME, J. Eng. Mater. Technol. 131 (2009) 021010-1/8.
[31] N. Gates, A. Fatemi, Notched fatigue behavior and stress analysis under multiaxial states of stress. Int. J. Fatigue 67 (2014) 2-14.
[32] L. Susmel, D. Taylor, An elasto-plastic reformulation of the Theory of Critical Distances to estimate lifetime of notched components failing in the low/medium-cycle fatigue regime. Trans. ASME, J. Eng. Mater. Technol. 132 (2010) 021002-1/8.
[33] L. Susmel, D. Taylor, Estimating lifetime of notched components subjected to variable amplitude fatigue loading according to the elasto-plastic Theory of Critical Distances. Trans. ASME, J. Eng. Mater. Technol. 137 (2015) 011008-1/15.
[34] N. Gates, A. Fatemi, Notch deformation and stress gradient effect in multiaxial fatigue. Theor. Appl. Fract. Mec. 84 (2016) 3-25.
[35] N.R. Gates, A. Fatemi, Multiaxial variable amplitude fatigue life analysis using the critical plane approach, Part II: Notched specimen experiments and life estimations. Int. J. Fatigue 106 (2018) 56-69.
[36] L. Susmel, D. Taylor, A novel formulation of the Theory of Critical Distances to estimate Lifetime of Notched Components in the Medium-Cycle Fatigue Regime. Fatigue Fract. Eng. Mater. Struct. 30 (2007) 567-581.
[37] L. Susmel, D. Taylor, The Modified Wöhler Curve Method applied along with the Theory of Critical Distances to estimate finite life of notched components subjected to complex multiaxial loading paths. Fatigue Fract. Eng. Mater. Struct. 31 (2008) 1047-1064.
[38] L. Susmel, D. Taylor, The Theory of Critical Distances to estimate lifetime of notched components subjected to variable amplitude uniaxial fatigue loading. Int. J. Fatigue 33 (2011) 900-911.
[39] L. Susmel, D. Taylor, A critical distance/plane method to estimate finite life of notched components under variable amplitude uniaxial/multiaxial fatigue loading. Int J Fatigue 38 (2012) 7-24.
[40] R. Louks, B. Gerin, J. Draper, H. Askes, L. Susmel, On the multiaxial fatigue assessment of complex three-dimensional stress concentrators. Int. J. Fatigue 63 (2014) 12-24.
[41] L. Susmel, G. Meneghetti, B. Atzori, A simple and efficient reformulation of the classical Manson-Coffin curve to predict lifetime under multiaxial fatigue loading. Part I: plain materials. Trans. ASME, J. Eng. Mater. Technol. 131 (2009) 021009-1/9.
[42] Y. Wang, L. Susmel, The Modified Manson-Coffin Curve Method to estimate fatigue lifetime under complex constant and variable amplitude multiaxial fatigue loading. Int. J. Fatigue 83 (2016) 135-149.
[43] L. Susmel, A simple and efficient numerical algorithm to determine the orientation of the critical plane in multiaxial fatigue problems. Int. J. Fatigue 32 (2010) 1875–1883.
[44] E. Macha, Simulation investigations of the position of fatigue fracture plane in materials with biaxial loads. Materialwiss Werkstofftech 20 (1989) 132–6.
[45] K. Kanazawa, K.J. Miller, M.W. Brown, Low-cycle fatigue under out-of phase loading conditions. Trans. ASME, J. Eng. Mater. Technol. 99 (1977) 222–228.
[46] M. Matsuishi, T. Endo, Fatigue of metals subjected to varying stress. Presented to the Japan Society of Mechanical Engineers, Fukuoka, Japan, 1968.
[47] S. D. Downing, D. F. Socie, Simple rainflow counting algorithms. Int. J. Fatigue 4 (1982) 31-40.
[48] R.P. Kaufman, T. Topper, The influence of static mean stresses applied normal to the maximum shear planes in multiaxial fatigue. In: Biaxial and Multiaxial fatigue and Fracture, Edited by A. Carpinteri, M. de Freitas and A. Spagnoli, Elsevier and ESIS, 2003, pp. 123-143.
[49] D.F. Socie, Fatigue damage models. Trans. ASME, J. Eng. Mater. Technol. 109 (1987) 293-298.
[50] L. Susmel, R. Tovo, P. Lazzarin, The mean stress effect on the high-cycle fatigue strength from a multiaxial fatigue point of view. Int. J. Fatigue 27 (2005) 928-943.
[51] L. Susmel, R. Tovo, D. Benasciutti, A novel engineering method based on the critical plane concept to estimate the lifetime of weldments subjected to variable amplitude multiaxial fatigue loading. Fatigue Fract. Eng. Mater. Struct. 32 (2009) 441-459.

[52] D.F. Socie, J. Morrow, Review of contemporary approaches to fatigue damage analysis, Risk and Failure Analysis for Improved Performance and Reliability, Edited by J. J. Burke & V. Weiss, Plenum Pub. Corp., New York, NY, USA, 1980, pp. 141–194.
[53] A. Palmgren, Die Lebensdauer von Kugellagern, Zeitschrift des Vereines Deutscher Ingenieure 68 (1924) 339–341.
[54] M.A. Miner, Cumulative damage in fatigue. J. Appl. Mech. 67 (1945) AI59–AI64.
[55] C.M. Sonsino, Fatigue testing under variable amplitude loading. Int. J. Fatigue 29 (2007) 1080–1089.
[56] W. D. Pilkey, D. F. Pilkey, Peterson's Stress Concentration Factors. Third Edition, Wiley, NY, USA, 2017.
[57] M. Zappalorto, P. Lazzarin, S. Filippi, Stress field equations for U and blunt V-shaped notches in axisymmetric shafts under torsion. Int. J. Fracture 164 (2010) 253-269.
[58] Y. Jiang, H. Sehitoglu, H., Modelling of Cyclic Ratchetting Plasticity—Part I: Development and Constitutive Relations. Trans. ASME, J. Appl. Mech. 63 (1996) 720–725.
[59] Y. Jiang, H. Sehitoglu, Modelling of Cyclic Ratchetting Plasticity—Part II: Comparison of Model Simulations With Experiments. Trans. ASME, J. Appl. Mech. 63 (1996) 726–733.
[60] J. Hoffmeyer, R. Döring, T. Seeger, M. Vormwald, Deformation behaviour, short crack growth and fatigue lives under multiaxial nonproportional loading. Int. J. Fatigue 28 (2006) 508–520.
[61] C. Han, X. Chen, K.S. Kim, Evaluation of multiaxial fatigue criteria under irregular loading. Int. J. Fatigue 24 (2002) 913-922.
[62] K. Kanazawa, K.J. Miller, M.W. Brown, Cyclic deformation of 1% Cr-No-V steel under out-of-phase loads. Fatigue Fract. Eng. Mater. Struct. 2 (1979) 217–228.
[63] D.G. Shang, G.Q. Sun, C.L. Yan, Multiaxial fatigue damage parameter and life prediction for medium-carbon steel based on the critical plane approach. Int. J. Fatigue 29 (2007) 2200–2207.
[64] K.S. Kim, J.C. Park, J.W. Lee, Multiaxial fatigue under variable amplitude loads. Trans. ASME, J. Eng. Mater. Technol. 121 (1999) 286-293.

List of Captions

Table 1. Summary of the experimental results generated by testing the plain specimens under strain control.

Table 2. Summary of the experimental results generated by testing under CA and VA fatigue loading the specimens containing the notches with r=1.5 mm.

Table 3. Summary of the experimental results generated by testing under CA and VA fatigue loading the specimens containing the notches with r=3 mm.

Table 4. Summary of the experimental results generated by testing under CA and VA fatigue loading the specimens containing the notches with r=6 mm.

Table 5. Summary of the experimental results generated by testing the notched specimens under VA fatigue loading where the axial and torsional loadings were applied at different frequencies.

Table 6. Static and fatigue properties of the materials used to investigate the accuracy of FE software ANSYS® in estimating stress path under time-variable elasto-plastic deformations.

Figure 1. Stress and strain components relative to the critical plane determined according to the γ-MVM under CA (c) and VA (d) fatigue loading.

Figure 2. The modified Manson-Coffin diagram (a); process zone defined according to the Theory of Critical Distances (b); determination of the critical distance L according to the Point Method (c).

Figure 3. The MMCCM applied along with the PM to estimate fatigue lifetime of notched components subjected to CA fatigue loading.

Figure 4. The MMCCM applied along with the PM to estimate fatigue lifetime of notched components subjected to VA fatigue loading.

Figure 5. Geometry of the plain and notched specimens being tested (a); experimental load spectrum (c, d); axial (d) and torsional (e) stabilised stress-strain curves; fully-reversed uniaxial (f) and torsional (g) Manson-Coffin curves.

Figure 6. Observed cracking behaviour.

Figure 7. Shear/axial strain paths used to assess the accuracy of FE software ANSYS® as well as of Jiang and Sehitoglu's method [58, 59] in estimating stress path under time-variable elasto-plastic deformations.

Figure 8. Three-dimensional FE models solved using commercial code ANSYS®.

Figure 9. Examples of the analyses carried out to assess the accuracy of FE software ANSYS® as well as of Jiang and Sehitoglu's method [58, 59] in estimating stress vs. strain loops under time-variable elasto-plastic deformations.

Figure 10. Examples showing the accuracy of FE code ANSYS® in modelling the stress vs. strain response of the tested plain specimens of carbon steel En8 (CA=Constant Amplitude; VA=Variable Amplitude; IPh=In-Phase; OoPh=90° Out-of-Phase; ZMS=Zero Mean Stress; N-ZMS=Non-Zero Mean Stress; f= ratio between the frequencies of the axial and torsional loading channels).

Figure 11. Overall accuracy of the proposed multiaxial fatigue life estimation technique (CA=Constant Amplitude; VA=Variable Amplitude; IPh=In-Phase; OoPh=90° Out-of-Phase; ZMS=Zero Mean Stress; N-ZMS=Non-Zero Mean Stress; f= ratio between the frequencies of the axial and torsional loading channels).

Tables

Code	R	$\varepsilon_{x,a\text{-}max}$	$\gamma_{xy,a\text{-}max}$	δ [°]	N_f [Cycles to failure]	Load History[(1)]
PSUCAZMS1	-1	0.0018			85408	CA
PSUCAZMS2		0.0019			71336	
PSUCAZMS3		0.0019			40132	
PSUCAZMS4		0.002			57039	
PSUCAZMS5		0.003			15040	
PSUCAZMS6		0.004			7338	
PSUCAZMS7		0.005			4059	
PSUCAZMS8		0.005			2251	
PSTCAZMS1	-1		0.0022		673052	CA
PSTCAZMS2			0.0035		54255	
PSTCAZMS3			0.0044		20705	
PSTCAZMS4			0.0046		14012	
PSTCAZMS5			0.0058		8247	
PSTCAZMS6			0.0068		6285	
PSTCAZMS7			0.0079		4003	
PSTCAZMS8			0.0094		3142	
PSBCAZMSIPh1	-1	0.0027	0.0046	0	8050	CA
PSBCAZMSOoPh2		0.0026	0.0045	90	1779	
PSBCANZMSIPh1	0	0.003	0.0046	0	5771	CA
PSBCANZMSOoPh2		0.0025	0.0039	90	1356	
PSBVAZMSIPh1	-1	0.005	0.0037	0	14936	VA
PSBVAZMSOoPh2		0.0037	0.0021	90	9986	
PSBVANZMSIPh1	0	0.0045	0.0035	0	10806	VA
PSBVANZMSOoPh2		0.0046	0.0025	90	8926	

[(1)]*CA=Constant Amplitude; VA=Variable Amplitude*

Table 1. Summary of the experimental results generated by testing the plain specimens under CA and VA fatigue loading.

Code	**R**	$F_{a\text{-}max}$ *[kN]*	$T_{a\text{-}max}$ *[Nm]*	δ *[°]*	N_f *[Cycles to failure]*	**Laod History**[(1)]
SNUCAZMS1	-1	78.7			6164	CA
SNUCAZMS2		58.3			35247	
SNUCAZMS3		52.0			41229	
SNUCAZMS4		69.8			13469	
SNUCAZMS5		46.8			8629	
SNUCAZMS6		42.3			145989	
SNBCAZMSIph1	-1	39.1	101.8	0	63012	CA
SNBCAZMSIph2		44.1	120.5	0	22974	
SNBCAZMSIph3		55.1	153.7	0	7156	
SNBCAZMSOoPh1	-1	41.3	110.6	90	31594	CA
SNBCAZMSOoPh2		45.1	125.6	90	11989	
SNBCAZMSOoPh3		55.8	158.1	90	6229	
SNBVAZMSIph1	-1	64.6	160.4	0	39428	VA
SNBVAZMSIph2		67.2	174.6	0	19519	
SNBVAZMSIph3		71.8	154.1	0	22811	
SNBVAZMSIph4		58.4	86.3	0	54296	
SNBVAZMSIph5		57.3	114.5	0	82054	
SNBVAZMSOut1	-1	65.6	117.9	90	50764	VA
SNBVAZMSIph2		67.7	130.3	90	35338	
SNBVAZMSOut3		72.9	128.9	90	22436	
SNBVAZMSOut4		55.2	99.4	90	67704	
SNBVAZMSOut5		56.4	132.1	90	78078	
SNBVANZMIph1	0	57.0	148.1	0	34677	VA
SNBVANZMIph2		60.5	157.2	0	25220	
SNBVANZMIph3		48.6	126.3	0	47235	
SNBVANZMIph4		68.4	177.7	0	12857	
SNBVANZMIph5		45.6	118.5	0	45245	
SNBVANZMOut1	0	57.0	148.1	90	62310	VA
SNBVANZMIph2		60.5	157.2	90	30665	
SNBVANZMOut3		48.6	126.3	90	58580	
SNBVANZMOut4		68.4	177.7	90	13755	
SNBVANZMOut5		45.6	118.5	90	116119	

[(1)]*CA=Constant Amplitude; VA=Variable Amplitude*

Table 2. Summary of the experimental results generated by testing under CA and VA fatigue loading the specimens containing the notches with r=1.5 mm.

Code	R	F_{a-max} [kN]	T_{a-max} [Nm]	δ [°]	N_f [Cycles to failure]	Laod History(1)
INBCAZMSIph1		40.4	102.72	0	156422	
INBCAZMSIph2	-1	49.0	123	0	47739	CA
INBCAZMSIph3		60.6	178.8	0	9725	
INBCAZMSOoPh1		46.0	140	90	46428	
INBCAZMSOoPh2	-1	51.0	132.5	90	33269	CA
INBCAZMSOoPh3		63.6	181.7	90	8428	
INBVAZMSIph1		66.7	153.1	0	39837	
INBVAZMSIph2		56.9	124.5	0	70645	
INBVAZMSIph3	-1	71.8	163.1	0	30919	VA
INBVAZMSIph4		79.5	184.7	0	24372	
INBVAZMSIph5		54.0	129.1	0	70879	
INBVAZMSOut1		64.5	176.4	90	32549	
INBVAZMSIph2		56.7	135.8	90	59743	
INBVAZMSOut3	-1	72.9	177	90	24930	VA
INBVAZMSOut4		77.2	197.9	90	19385	
INBVAZMSOut5		54.3	132.9	90	65910	
INBVANZMIph1		55.1	143.2	0	77310	
INBVANZMIph2		60.6	157.4	0	39124	
INBVANZMIph3	0	66.7	173.3	0	37870	VA
INBVANZMIph4		73.4	190.7	0	25609	
INBVANZMIph5		80.8	209.9	0	9559	
INBVANZMOut1		55.1	143.2	90	99157	
INBVANZMIph2		60.6	157.4	90	45491	
INBVANZMOut3	0	66.7	173.3	90	28616	VA
INBVANZMOut4		73.4	190.7	90	20810	
INBVANZMOut5		80.8	209.9	90	10386	

(1)*CA=Constant Amplitude; VA=Variable Amplitude*

Table 3. Summary of the experimental results generated by testing under CA and VA fatigue loading the specimens containing the notches with r=3 mm.

Code	R	$F_{a\text{-}max}$ *[kN]*	$T_{a\text{-}max}$ *[Nm]*	δ *[°]*	N_f *[Cycles to failure]*	Laod History(1)
BNBCAZMSIph1		39.3	114.8	0	225655	
BNBCAZMSIph2	-1	49.8	126.3	0	58662	CA
BNBCAZMSIph3		67.2	170.7	0	12423	
BNBCAZMSOoPh1		49.6	114.2	90	131784	
BNBCAZMSOoPh2	-1	61.8	148.4	90	35127	CA
BNBCAZMSOoPh3		69.5	186.5	90	14146	
BNBVAZMSIph1		80.6	209.5	0	33765	
BNBVAZMSIph2		88.7	230.4	0	15386	
BNBVAZMSIph3	-1	72.6	188.6	0	52223	VA
BNBVAZMSIph4		65.3	169.8	0	97300	
BNBVAZMSIph5		95.0	246.8	0	14169	
BNBVAZMSOut1		80.6	209.5	90	36032	
BNBVAZMSIph2		88.7	230.4	90	15681	
BNBVAZMSOut3	-1	72.6	188.6	90	51710	VA
BNBVAZMSOut4		65.3	169.8	90	75650	
BNBVAZMSOut5		95.0	246.8	90	12223	
BNBVANZMIph1		65.0	168.9	0	39870	
BNBVANZMIph2		71.5	185.8	0	29100	
BNBVANZMIph3	0	78.7	204.5	0	10486	VA
BNBVANZMIph4		59.8	155.4	0	62620	
BNBVANZMIph5		67.9	176.4	0	35225	
BNBVANZMOut1		65.0	168.9	90	50072	
BNBVANZMIph2		71.5	185.8	90	27149	
BNBVANZMOut3	0	78.7	204.5	90	28250	VA
BNBVANZMOut4		59.8	155.4	90	61250	
BNBVANZMOut5		67.9	176.4	90	46328	

(1)*CA=Constant Amplitude; VA=Variable Amplitude*

Table 4. Summary of the experimental results generated by testing under CA and VA fatigue loading the specimens containing the notches with r=6 mm.

Code	r [mm]	R	$F_{a\text{-}max}$ [kN]	$T_{a\text{-}max}$ [Nm]	f	N_b [Blocks to failure]
SNBVAZMSDF1	1.5	-1	70.0	181.9	0.5	53
SNBVAZMSDF2			64.4	167.3		69
SNBVAZMSDF3			58.0	150.6		76
SNBVAZMSDF4			52.1	135.4		179
SNBVAZMSDF5	1.5	-1	70.0	181.9	2	217
SNBVAZMSDF6			64.4	167.3		344
SNBVAZMSDF7			58.0	150.6		647
SNBVAZMSDF8			77.0	200.1		148
INBVAZMSDF1	3	-1	70.0	181.9	0.5	96
INBVAZMSDF2			64.4	167.3		132
INBVAZMSDF3			58.0	150.6		163
INBVAZMSDF4			52.1	135.4		280
INBVAZMSDF5	3	-1	70.0	181.9	2	278
INBVAZMSDF6			64.4	167.3		510
INBVAZMSDF7			58.0	150.6		786
INBVAZMSDF8			77.0	200.1		252
BNBVAZMSDF1	6	-1	70.0	181.9	0.5	162
BNBVAZMSDF2			64.4	167.3		163
BNBVAZMSDF3			58.0	150.6		291
BNBVAZMSDF4			77.0	200.1		72
BNBVAZMSDF5	6	-1	70.0	181.9	2	780
BNBVAZMSDF6			64.4	167.3		813
BNBVAZMSDF7			77.0	200.1		565
BNBVAZMSDF8			84.7	220.1		240

Table 5. Summary of the experimental results generated by testing the notched specimens under VA fatigue loading where the axial and torsional loadings were applied at different frequencies.

	AISI304 [49]	**S46N** [60]	**SNCM630** [61]	**1%Cr-Mo-V** [62]	**45 Steel** [63]	**S45C** [64]
Outer/inner diameter *[mm]*	16/15	41/36	12.5/10	22/16	25/21	12.5/10
E *[GPa]*	183	200	196	200	190	186
G *[GPa]*	83	77	77	77	79	71
ν_e	0.3	0.3	0.273	0.3	0.202	0.28
σ_y *[MPa]*	325	365	951	707	370	496
σ_{UTS} *[MPa]*	650		1103	805	610	770
σ'_f *[MPa]*	1000	865	1272	987	843	923
b	-0.114	-0.097	-0.073	-0.071	-0.1047	-0.099
ε'_f	0.171	0.119	1.54	1.369	0.3269	0.359
c	-0.402	-0.359	-0.823	-0.802	-0.5458	-0.519
K' *[MPa]*	1660	1329	1056	1113	1258	1215
n'	0.287	0.244	0.054	0.11	0.208	0.217
τ'_f *[MPa]*	709	500	858	570	559	685
b_o	-0.121	-0.097	-0.061	-0.071	-0.1078	-0.12
γ'_f	0.413	0.206	1.51	2.371	0.496	0.198
c_o	-0.353	-0.359	-0.706	-0.802	-0.469	-0.36
K'_o *[MPa]*	785	785		592		
n'_o	0.296	0.296		0.05		
K'_{NP} *[MPa]*	2075	1161	1320	1391	1573	1519
n'_{NP}	0.287	0.244	0.054	0.11	0.208	0.217

Table 6. Static and fatigue properties of the materials used to investigate the accuracy of FE software ANSYS® in estimating stress path under time-variable elasto-plastic deformations.

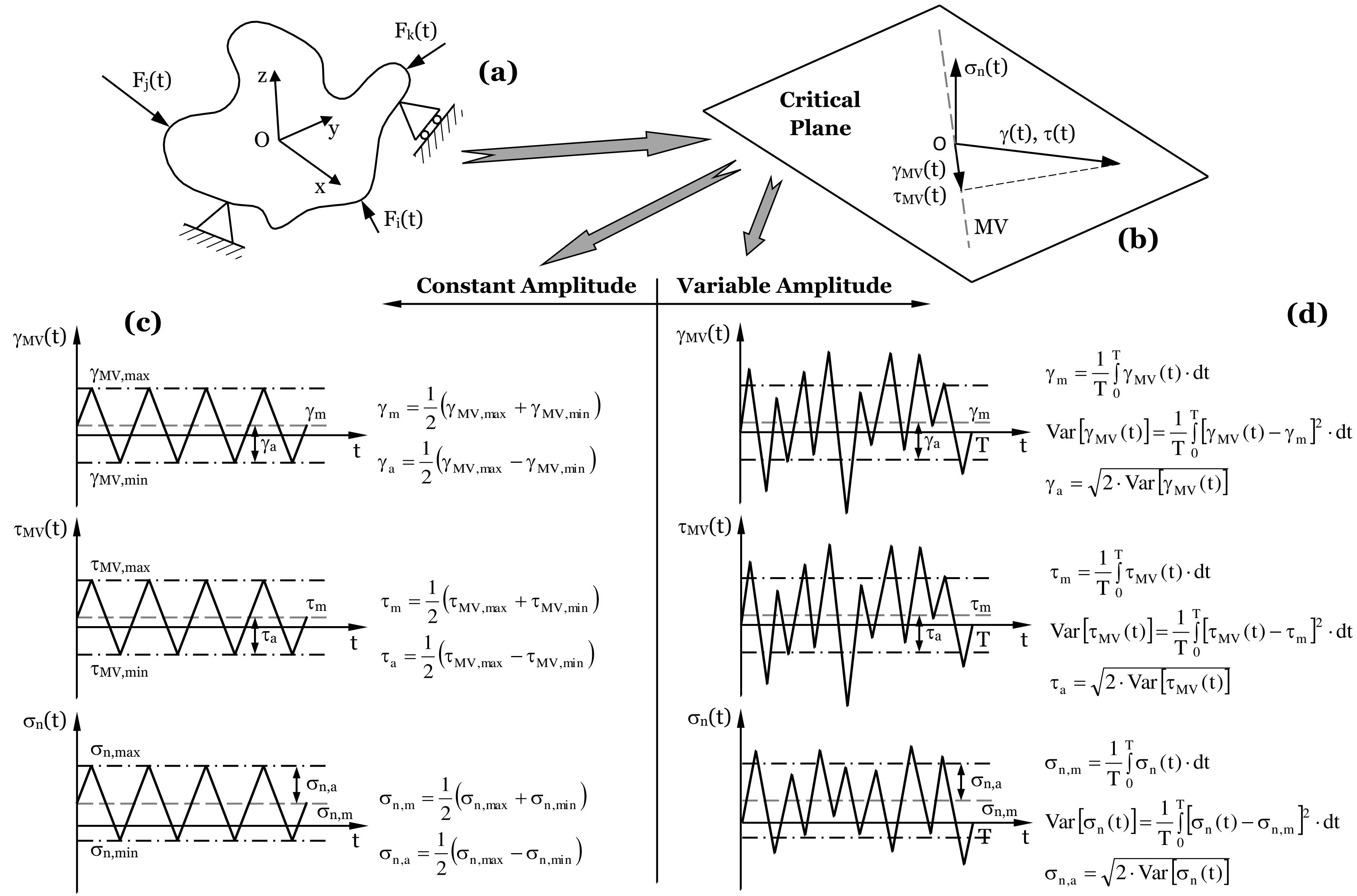

Figure 1. Stress and strain components relative to the critical plane determined according to the γ-MVM under CA (c) and VA (d) fatigue loading.

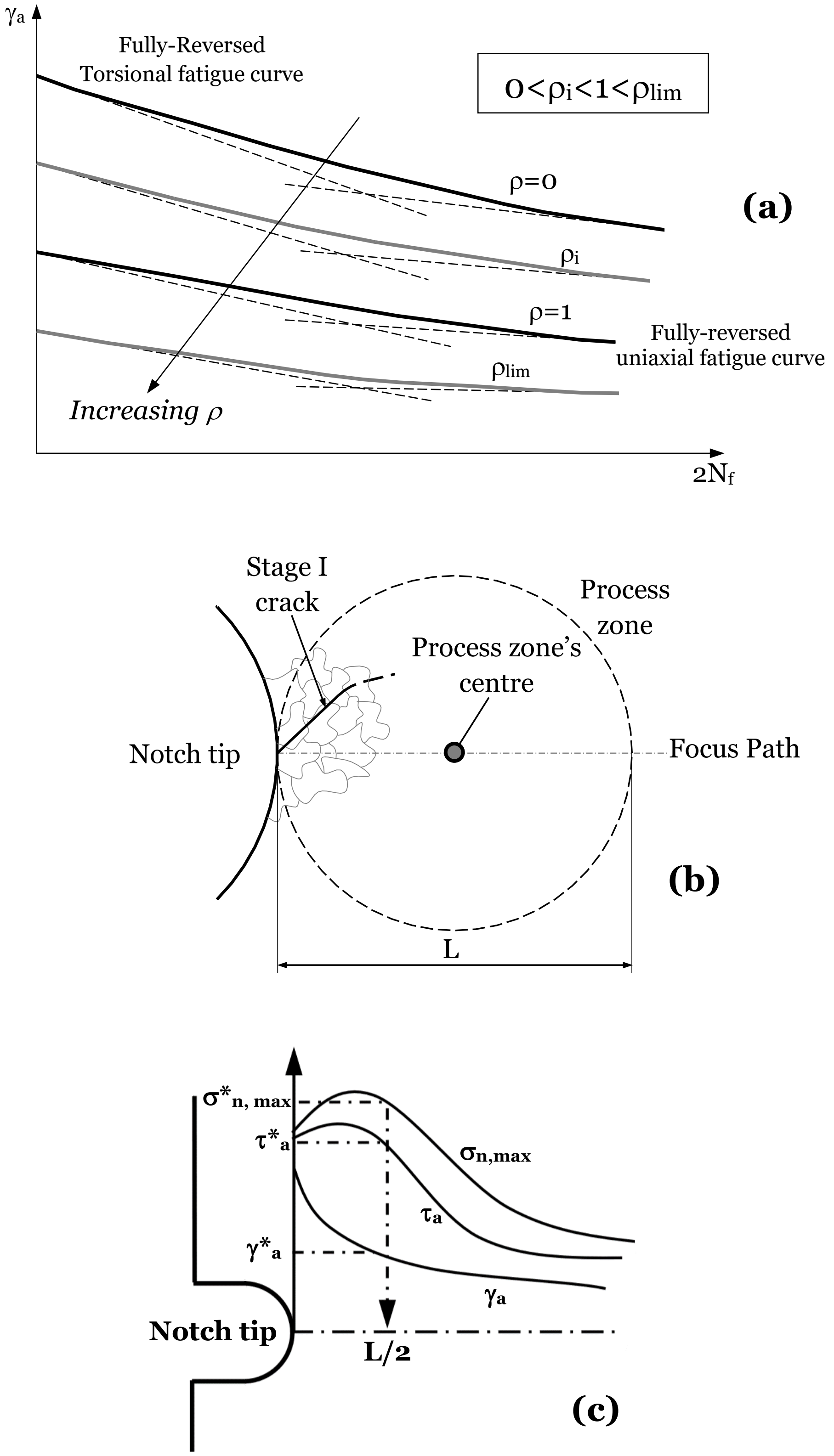

Figure 2. The modified Manson-Coffin diagram (a); process zone defined according to the Theory of Critical Distances (b); determination of the critical distance L according to the Point Method (c).

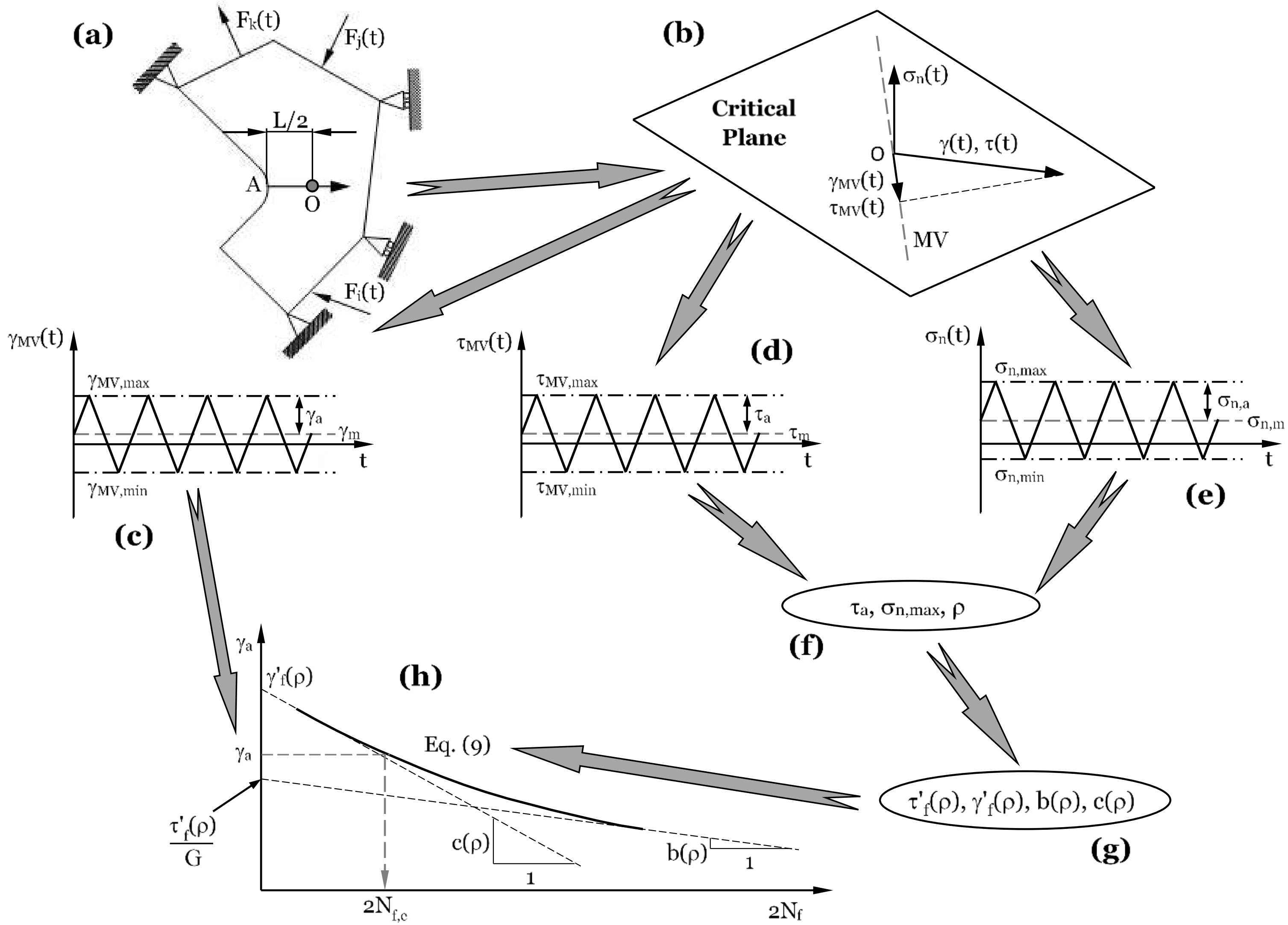

Figure 3. The MMCCM applied along with the PM to estimate fatigue lifetime of notched components subjected to CA fatigue loading.

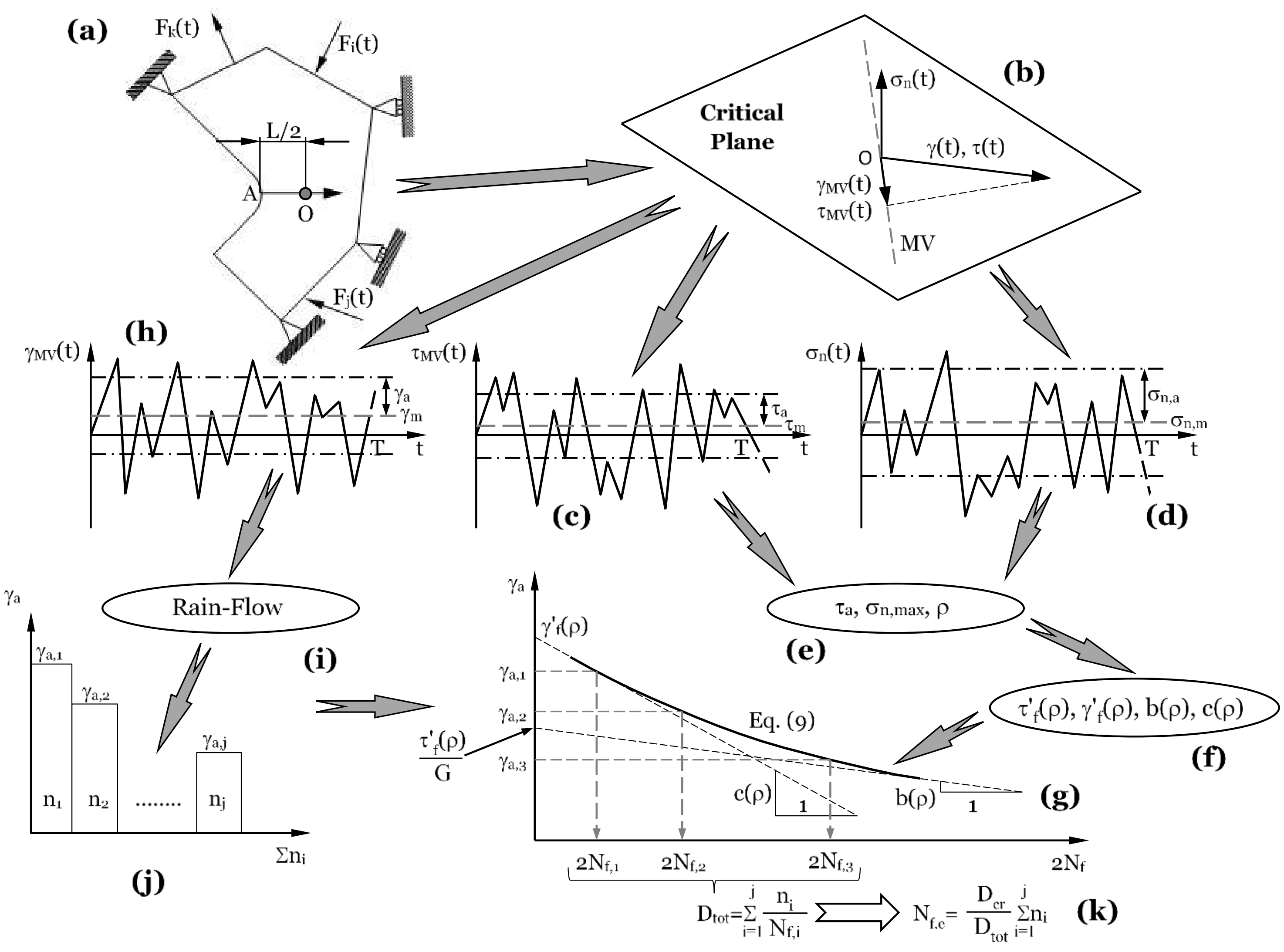

Figure 4. The MMCCM applied along with the PM to estimate fatigue lifetime of notched components subjected to VA fatigue loading.

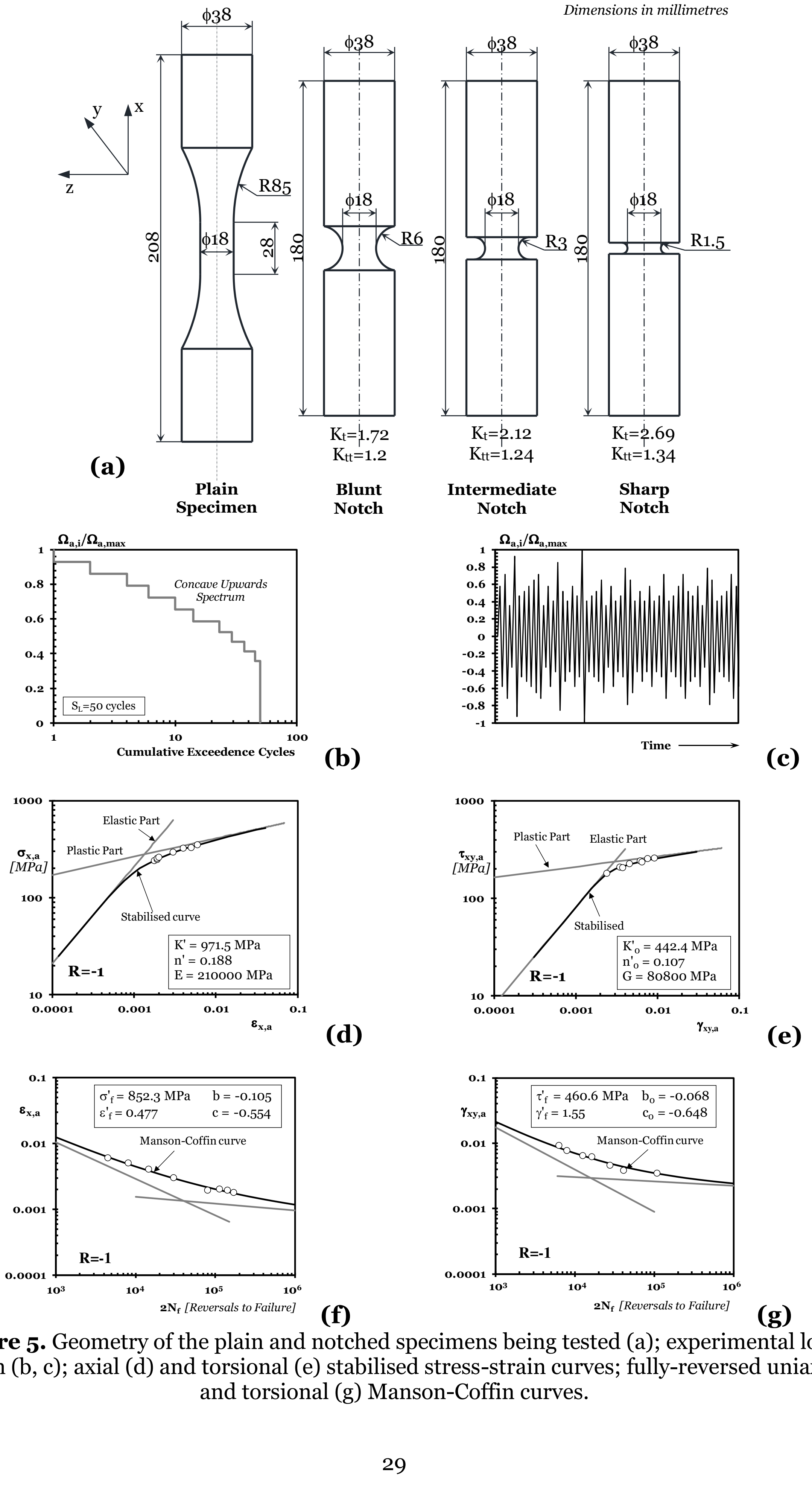

Figure 5. Geometry of the plain and notched specimens being tested (a); experimental load spectrum (b, c); axial (d) and torsional (e) stabilised stress-strain curves; fully-reversed uniaxial (f) and torsional (g) Manson-Coffin curves.

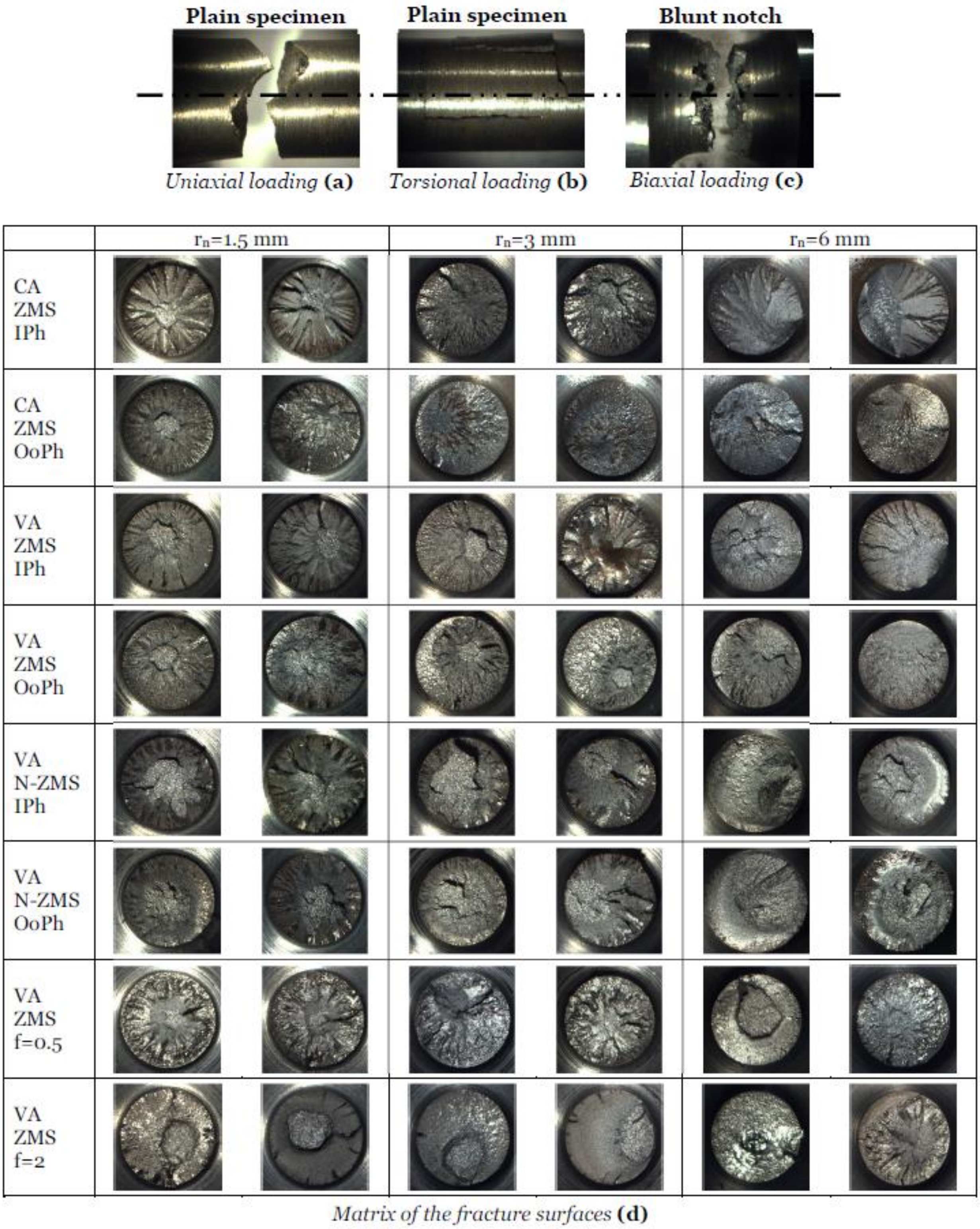

Figure 6. Observed cracking behaviour.

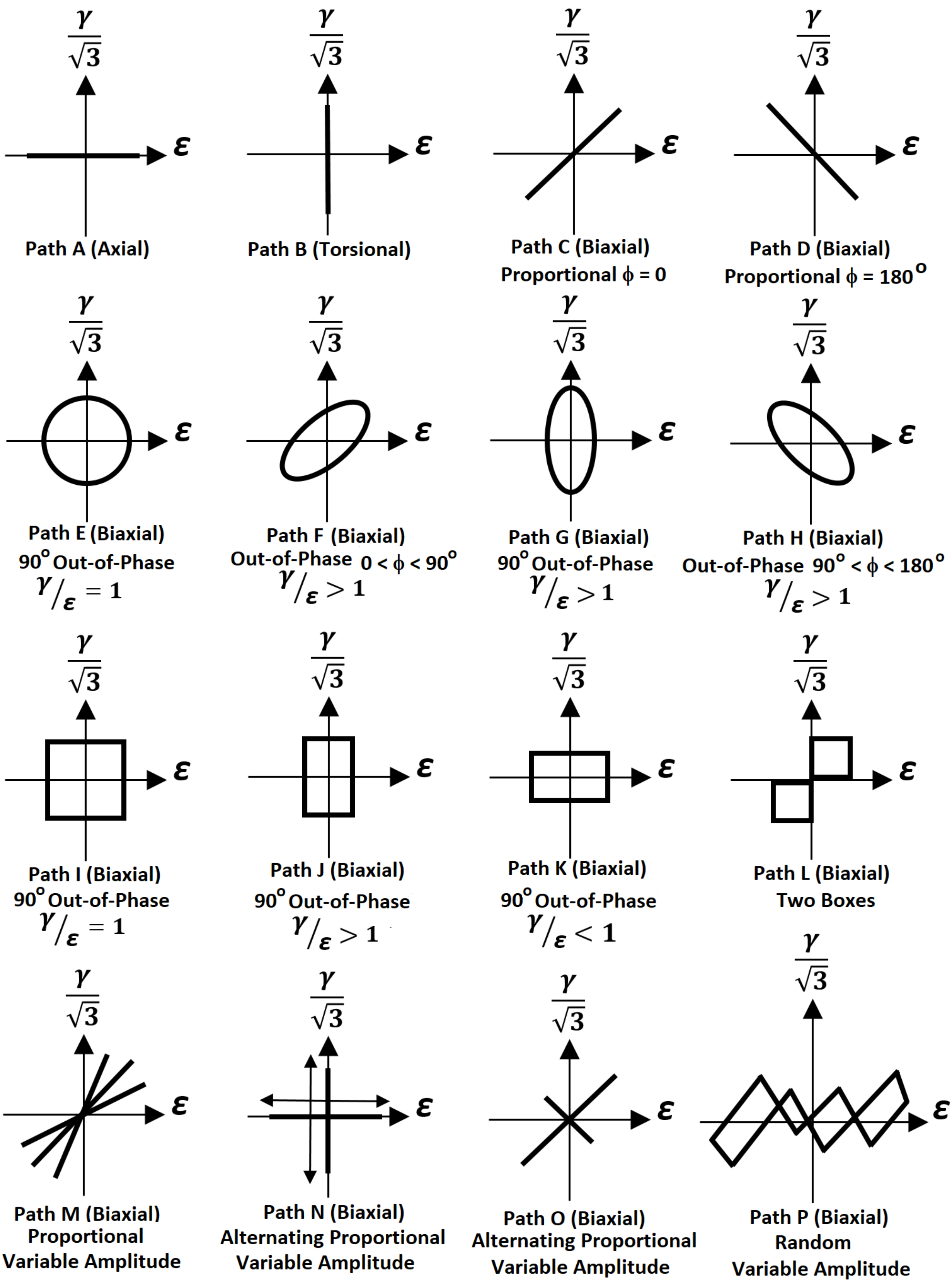

Figure 7. Shear/axial strain paths used to assess the accuracy of FE software ANSYS® as well as of Jiang and Sehitoglu's method [58, 59] in estimating stress path under time-variable elasto-plastic deformations.

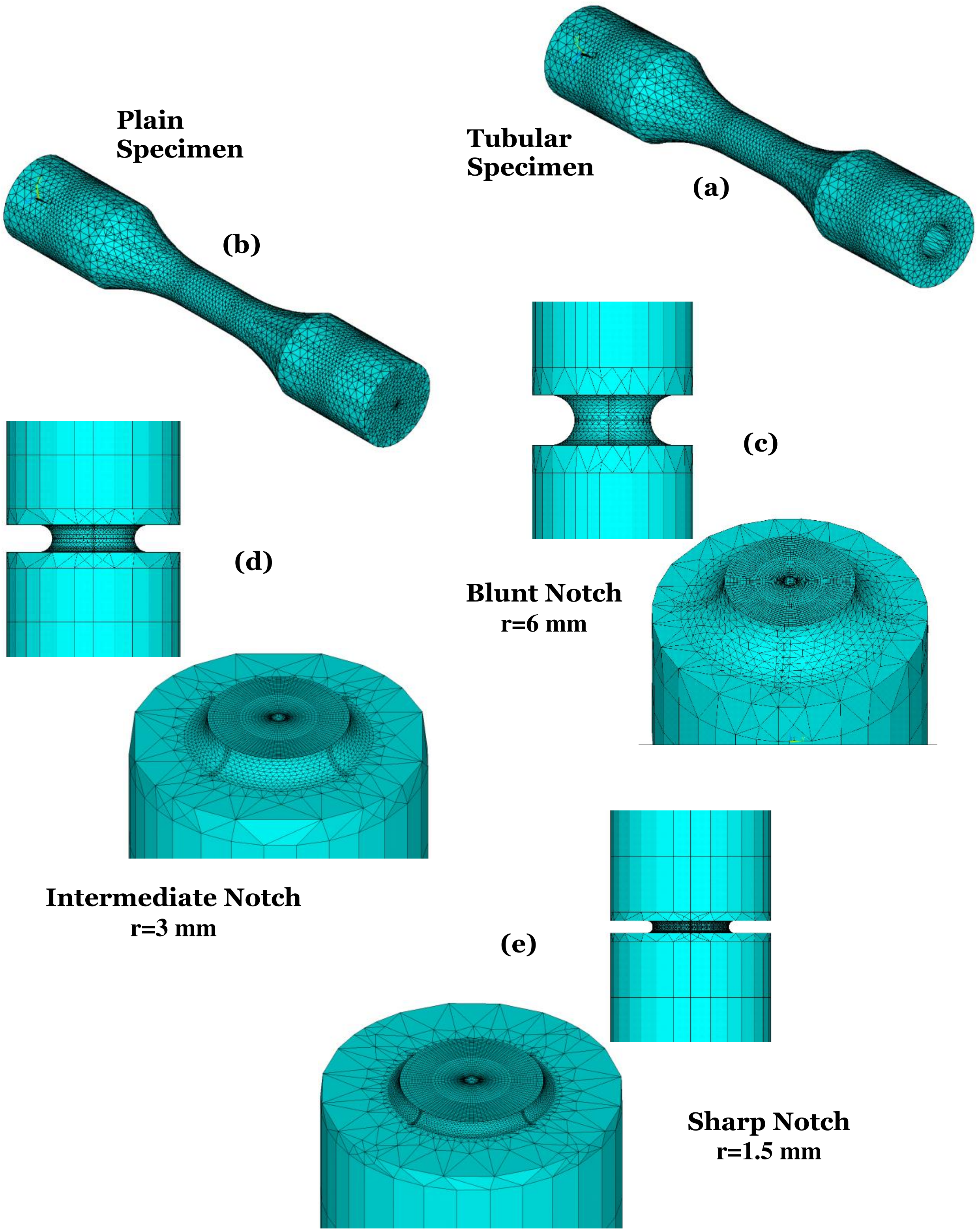

Figure 8. Three-dimensional FE models solved using commercial code ANSYS®.

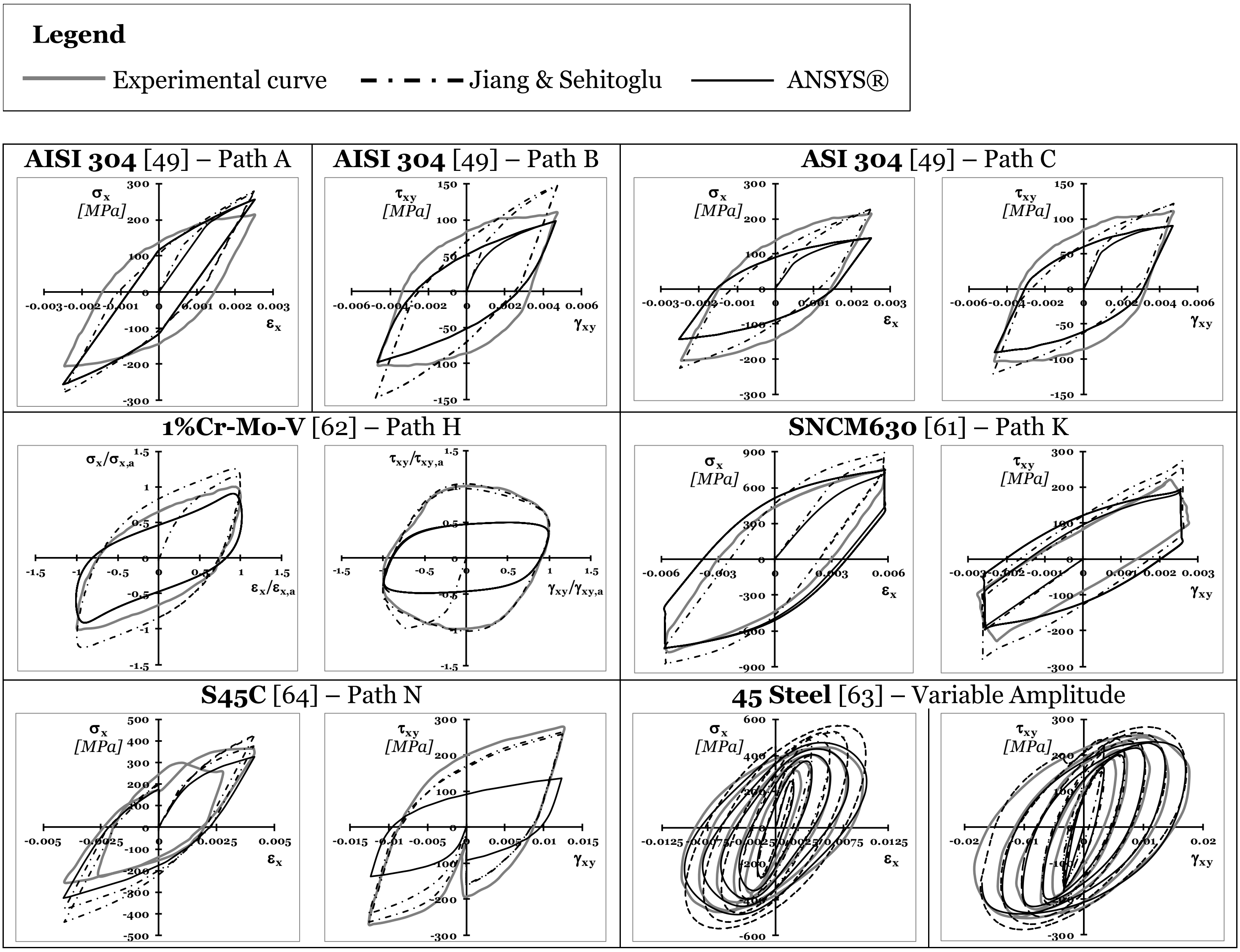

Figure 9. Examples of the analyses carried out to assess the accuracy of FE software ANSYS® as well as of Jiang and Sehitoglu's method [58, 59] in estimating stress vs. strain loops under time-variable elasto-plastic deformations.

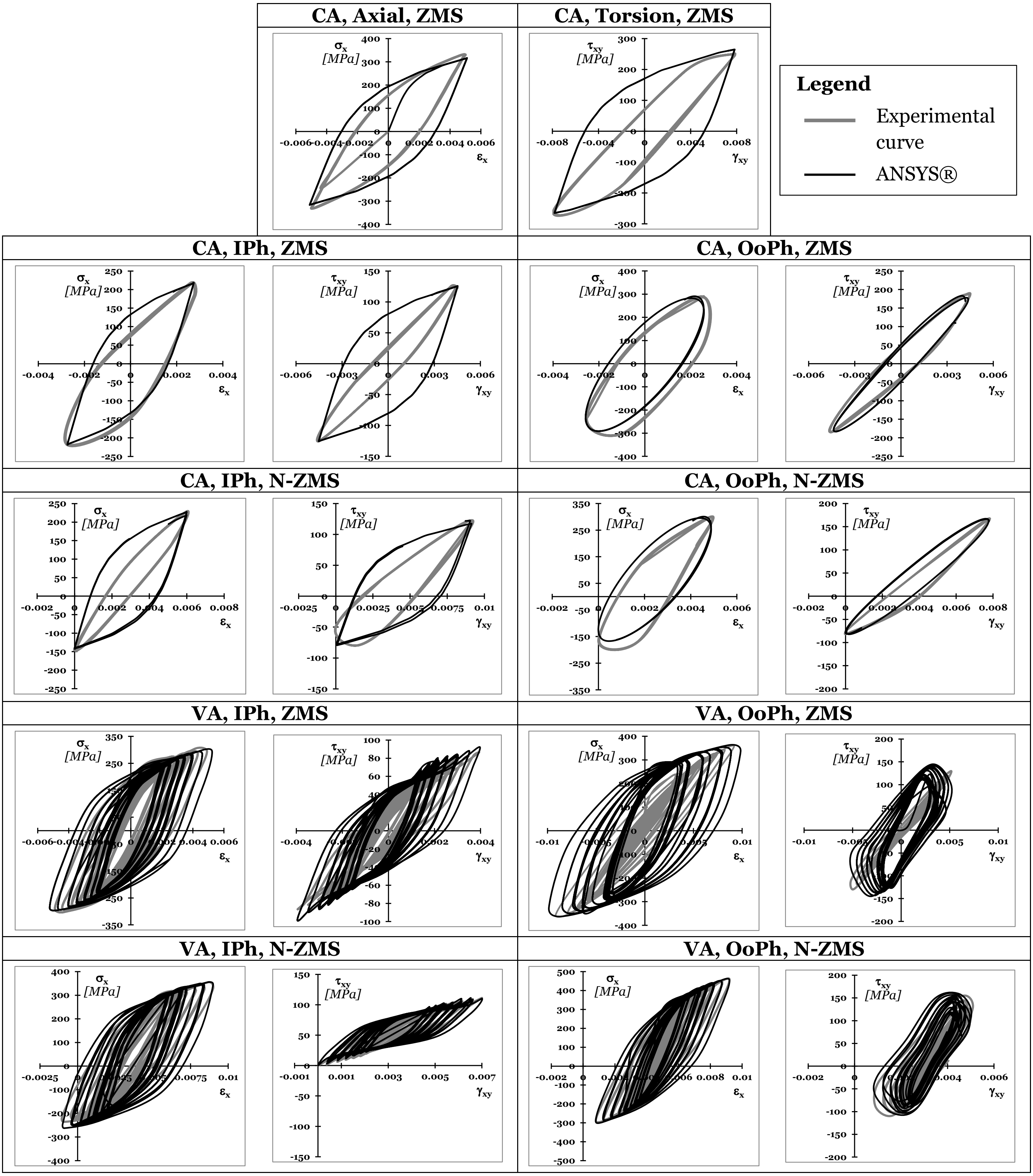

Figure 10. Accuracy of FE code ANSYS® in modelling the stress vs. strain response of the tested plain specimens of carbon steel En8 (CA=Constant Amplitude; VA=Variable Amplitude; IPh=In-Phase; OoPh=90° Out-of-Phase; ZMS=Zero Mean Stress; N-ZMS=Non-Zero Mean Stress).

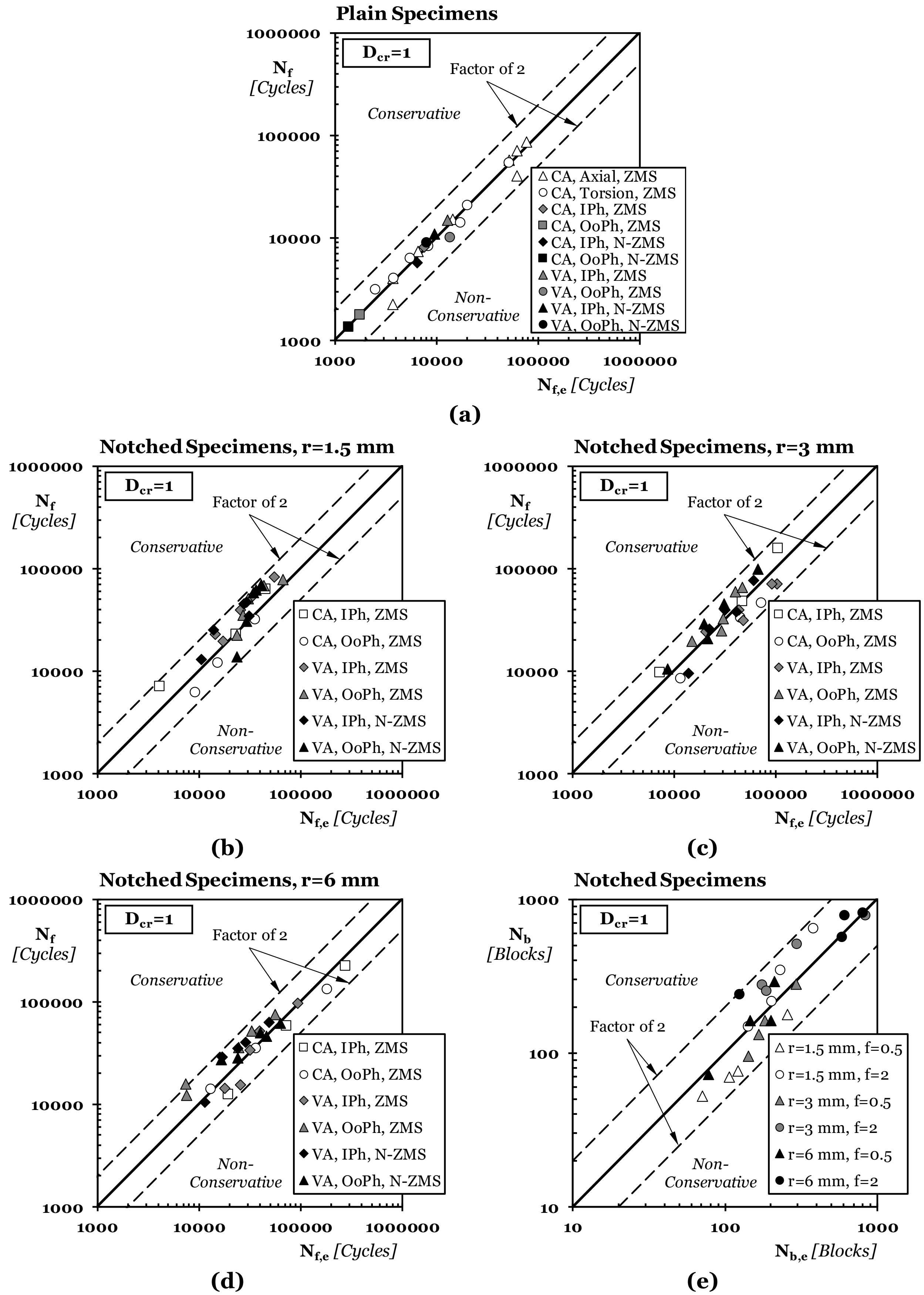

Figure 11. Overall accuracy of the proposed multiaxial fatigue life estimation technique (CA=Constant Amplitude; VA=Variable Amplitude; IPh=In-Phase; OoPh=90° Out-of-Phase; ZMS=Zero Mean Stress; N-ZMS=Non-Zero Mean Stress; f= ratio between the frequencies of the axial and torsional loading channels).